10 Copies
NAA
9-28-66

~~UNCLASSIFIED~~

NAA-SR-11397

COPY

99 PAGES

Classification cancelled
by authority of TID-1389-52
by EB DTIC, date 2-2-77
Exempt from CCRP Re-review Requirement
(per 7/22/82 Duff/Caudle memorandum)
HA 3/8/04

SNAP 10A FS-3
REACTOR PERFORMANCE
(Title Unclassified)

AEC Research and Development Report

~~RESTRICTED DATA~~

GROUP 1
Excluded from automatic downgrading and declassification

ATOMICS INTERNATIONAL
A DIVISION OF NORTH AMERICAN AVIATION, INC.

~~CONFIDENTIAL~~

DISCLAIMER

LEGAL NOTICE

Printed in USA Price $2.45 Available from the

U.S. Atomic Energy Commission,
Division of Technical Information Extension,
P. O. Box 62
Oak Ridge, Tennessee.

Please direct to the same address inquiries covering the procurement of other classified AEC reports.

~~UNCLASSIFIED~~

NAA-SR-11397
~~NAA-SR-11397~~
~~SNAP REACTOR~~,
SNAP PROGRAM
M-3679 (45th Ed.)

SNAP 10A FS-3

REACTOR PERFORMANCE

(Title Unclassified)

By

J. P. HAWLEY
R. A. JOHNSON

Exempt from CCRP Re-review Require
(per 7/22/82 Duff/Caudle memorand
HA 3/4/

TID-1389-52
EB 2/2/77

~~RESTRICTED DATA~~

~~This document contains restricted data as defined in the Atomic Energy Act of 1954. Its transmittal or the disclosure of its contents in any manner to an unauthorized person is prohibited.~~

~~This document contains Confidential Restricted Data relating to National applications of atomic energy.~~

ATOMICS INTERNATIONAL

A DIVISION OF NORTH AMERICAN AVIATION, INC.
P.O. BOX 309 CANOGA PARK, CALIFORNIA

EB

[illegible] THIS DOCUMENT IS UNLIMITED

CONTRACT: AT(11-1)-GEN-8
ISSUED: AUGUST 15, 1966

~~CONFIDENTIAL~~

[illegible]

DISTRIBUTION

SYSTEMS FOR NUCLEAR AUXILIARY POWER (SNAP)-REACTOR SNAP PROGRAM
M-3679 (45th Ed.)

	No. of Copies
AEC Patent Office	1
Aerojet-General Corporation (NASA)	6
Aerojet-General Corporation, Sacramento	1
Aerojet-General Nucleonics (NASA)	1
Aeronautical Systems Division	2
Aerospace Corporation	1
Air Force Foreign Technology Division	1
Air Force Headquarters	1
Air Force Surgeon General	1
Air Force Technical Applications Center	1
Air Force Weapons Laboratory	3
Air University Library	1
AiResearch Manufacturing Company, Phoenix	1
Allison Division-GMC	1
Argonne National Laboratory	1
Army Ballistic Research Laboratories	1
Army Director of Transportation	1
ARO, Inc.	1
Battelle Memorial Institute	1
Battelle-Northwest	2
Bendix Corporation (NASA)	1
Brookhaven National Laboratory	1
Bureau of Naval Weapons	2
Bureau of Ships	2
California Patent Group	1
Central Intelligence Agency	1
Chicago Patent Group	1
Director of Defense Research and Engineering	1
Douglas Aircraft Company, Inc., Newport Beach	1
DuPont Company, Aiken	1
DuPont Company, Wilmington	1
Electro-Optical Systems, Inc.	1
General Atomic Division	1
General Dynamics/Convair (AF)	1
General Dynamics/Fort Worth	1
General Electric Company, Cincinnati	1
General Electric Company (FPD)	2
General Electric Company (MSVD)	1
General Electric Company, San Jose	2
Hughes Research Laboratories	1
Institute for Defense Analyses	1
Jet Propulsion Laboratory	2
Johns Hopkins University (APL)	1
Lockheed-Georgia Company	1
Los Alamos Scientific Laboratory	1
Minnesota Mining and Manufacturing Company	1
Monsanto Research Corp.	1
Mound Laboratory	1
NASA Ames Research Center	1
NASA Goddard Space Flight Center	2
NASA Lewis Research Center	7
NASA Manned Spacecraft Center	1
NASA Marshall Space Flight Center	3
NASA Scientific and T Information Facility	
National Aeronautics Administration, Wa	
National Reactor Tes	
Naval Air Developme	
Naval Radiological D	
Naval Research Lab	
Navy Marine Engine	
New York Operatior	
Nuclear Weapons T Pacific	
Oak Ridge Operatio	
Office of Naval Res	
Office of the Chief	
Office of the Chief	
Office of the Chief (OP-03EG)	
Pratt and Whitney (NASA)	
Rand Corporation	
Radio Corporatio	
Sandia Corporati	
Union Carbide Co	
University of Cal	
Westinghouse El	
Westinghouse Electric Corpora... (AF)	1
Westinghouse Electric Corporation (NASA)	1
Westinghouse Electric Corporation (WAL)	1
White Sands Missile Range	2
Division of Technical Information Extension	10
AI Library (Includes 2 copies to CPAO, 2 copies to AEC, Washington, 2 copies to SFOO)	43

Do not reproduce

UNCLASSIFIED

CONTENTS

CONTENTS

TABLES

FIGURES

FIGURES

ABSTRACT

SNAP 10FS-3 was the first flight-qualified SNAP reactor system to be operated in a simulated space environment. Pre-startup qualification testing, automatic startup, endurance period performance, extended operation test and reactor shutdown are described as they affected, or were affected by, overall reactor performance. Performance of the reactor control system and the diagnostic instrumentation is critically evaluated.

I. INTRODUCTION AND SUMMARY

On January 22, 1965, the SNAP 10A nuclear ground test system was brought to full power as the start of the endurance test. This system, designated S10FS-3, is identical to the SNAP 10A system flight-tested in April of 1965[1, 2] except for minor modifications made to accommodate ground safety and facility requirements. This was the first operation of a flight-qualified reactor in the SNAP program. A preliminary report of S10FS-3 results is available.[3]

Prior to initiation of the automatic startup procedure, the coarse control drums were driven to the full-in position by stepper motors rather than being inserted by snap-in springs immediately after receipt of the startup command. The startup command was given at 7:00 a. m. at which time the fine control drums began stepping in at the rate of 0.5°/150 sec. The startup proceeded normally with less than 7% of the control drum steps having a step time interval different from the nominal 150 sec. The transient performance, that followed sensible heat at 12:58 p. m., was very close to the prediction. The temperature ramp following the initial transient was 6 to 7°F/min which is slightly higher than predicted. Initial closure of the temperature switch occurred at 1054°F terminating continuous controller operation at 3:02 p. m.

The temperature then drifted downward until the temperature switch reopened at 1023°F, allowing the controller to insert more reactivity. Two drum steps were inserted prior to the switch reclosing, and this behavior became typical during the active control period. The apparent reason for the two steps is the slow response of the sensor to changes in NaK temperature. The sensor's temperature does not increase sufficiently to close the switch in the 150 sec time between steps. Because the temperature switch set point was about 20°F higher than expected, causing peak temperatures above 1060°F following a double step, the set point was readjusted to near 1010°F following the second double step. After set point adjustment all steps occurred when the temperature dropped to 1007 ± 1°F.

The reactivity insertion rate was higher than predicted during the first 15 to 20 hr after reaching full power but was close to the prediction for the remainder of the active control period. The higher-than-expected heating rate during the approach to power and the higher-than-expected reactivity loss rate during the

first few hours of power operation have been attributed to abnormal reflector movement. To allow for remote handling of the reflector halves, the support hinges had been modified for this test and indications are that reflector half movement was caused by differential expansion between the reflector and vessel. The most definite indication of this effect was the actuation of both reflector ejection limit switches shortly after the start of heatup. Thermal and mechanical analysis of the reflector motion in FS-3 is provided in Appendix A.

After 72 hr of active control, the controller was deenergized. At this time, the average NaK temperature in the core was 973°F. During the initial week of statically controlled operation, reactor behavior was very similar to that previously predicted. Approximately 2 weeks after the beginning of static control, the average coolant temperature was above the nominally predicted value but was decreasing at a higher rate than predicted. This rate of decrease continued and after approximately 5 weeks of operation the average core temperature dropped below the predicted nominal value. However, the rate of temperature decrease was observed to diminish with time. Average coolant temperature at the end of one full year of operation was 908°F. The nominal predicted year-end average coolant temperature was 945°F with a possible minimum of 905°F.

It appears that the coolant temperature deviation from nominal behavior was primarily due to continuing hydrogen redistribution. Prepoison burnout, hydrogen leakage, fuel burnup and fission product accumulation, radiation damage effects in the shield, fuel, and beryllium reflector, and thermal effects associated with fuel thermal conductance also introduce some uncertainty in the reactivity performance analysis. In addition, a reactivity effect has been attributed to the special ground test requirement for reflector mounting on FS-3 which allowed reflector movement.

From the FS-3 test results, an analytical model has been developed which considers all known reactivity effects in the calculation of SNAP 10A reactor performance. A good match to the observed reactor performance has been obtained using this model with reasonable values for all reactivity effects. The model will be useful in analyzing future SNAP reactor static control period performance.

Due to the observed departure from anticipated FS-3 behavior, the static control characteristics of FS-4 became more significant. It was noted[1, 2] that the reactor temperature drift, when corrected for the small temperature difference, was almost the same as that observed on FS-3. This is a definite indication that like SNAP reactors will behave in a similar manner. This information, even though obtained during a period of relatively rapid temperature change, is significant since it verifies that behavior of statically controlled SNAP-type reactors can be predicted based on ground test operations.

In January 1966, the USAEC granted permission to increase the reactor power level and to continue to test S10FS-3 beyond the originally planned 1-yr operating period. After 390 days of continuous full power operation reactivity was inserted to increase reactor power to 44 kw. Active control was employed for 3 days, followed by an additional 25 days of static control. The control and diagnostic instrumentation systems functioned in a normal manner during the extended operation test, despite the year-long static control period which preceded the power level increase. Reactor performance at higher temperature conditions indicated that the hydrogen loss rate from the fuel elements was not significantly greater than predicted. S10FS-3 reactor operation was continued through March 15, 1966, and the system was shut down after more than 10,000-hr uninterrupted operation at full power.

As a result of FS-3 and FS-4 operational data, a study was undertaken to evaluate the effect of this new information on the performance of high-temperature, high-power, statically controlled reactors. This study revealed that the magnitude of the temperature uncertainties associated with these reactors will not be proportionally greater than the uncertainties at SNAP 10A conditions for several reasons. The hydrogen redistribution effect is essentially completed during the active control period for high-temperature reactors; all uncertainties are reduced by the strong temperature dependency of the overriding high-temperature reactivity loss mechanism – hydrogen leakage. Prepoison loading uncertainties are reduced due to the larger amount of poison required for the higher powered conditions. For these reasons the uncertainties are held within the range where static control is feasible. Because of the close relationship of FS-3 to this study, it is discussed in Appendix B of this report.

BLANK

II. S10FS-3 HISTORY PRIOR TO STARTUP

All components for the FS-3 reactor went through formal reactor assembly and system acceptance tests. These tests included both thermal-vacuum and vibration tests. The reactivity worth of the fuel elements was checked in the SCA-4 critical assembly both before and after application of the hydrogen barrier coating containing samarium. Following this check, the fuel was subject to an acceptance vibration test and a hydrogen permeation test.

The FS-3 system was loaded with dummy fuel elements and subjected to a 5 min qualification level vibration test, following the acceptance vibration test, to simulate launch conditions. The fuel elements were given a separate 5 min qualification level vibration test and again permeation-tested prior to loading. No significant change in leak rate resulted from the qualification level vibration test.

The fuel and NaK were loaded in FS-3 at the Santa Susana nuclear ground test facility (Building 024). The reflector assembly was modified for the endurance test. Modifications included the installation of the flight drives on the fine control drums and modified flight drives on the coarse control drums in place of the snap-in springs. The reflector support hinges were modified to allow remote handling, the ejection springs were modified so that they exerted no force, a sash weight was attached to each reflector half to provide the ejection force, and the retainer band was modified to incorporate a retractable pin in place of one of the rivets.

The complete system was subjected to four thermal cycles (using electrical heaters) to temperatures of 800 to 870°F. Heat rates were nominally held to below 5°F/min during these tests. In addition to these thermal cycles, the system had been heated to 735°F during NaK loading. Nuclear temperature defect data and temperature sensor resistance data were extrapolated from the 870°F level to the operating level above 1000°F.

On January 21, the day before the start of the endurance test, the control drums were inserted at the rate of 1 step each 300 sec until the transient following sensible heat had occurred. The purpose of this test was to verify the analytical predictions prior to subjecting the system to the faster design startup rate. The transient reached a peak power of 12.7 kwt and an outlet

temperature of 216°F. The maximum heating rate encountered was 0.77°F/sec. As these results were close to the prediction, approval was given to proceed with the endurance test.

Radioactivity generated by the slow stepping rate startup decayed so that the multiplied source power level at the start of the test on January 22 was 5.6×10^{-7} kw, slightly higher than the 10^{-10} to 10^{-8} kw anticipated for the space source power.

III. STARTUP PERIOD

A. CONTROL SYSTEM PERFORMANCE

The SNAP 10A reactor control system consists of a controller, control drum actuators, temperature detectors, and temperature switches. Whenever the controller is energized and receives a low-temperature input signal, it will develop output signals to drive the 2 fine control drum actuators in parallel at the rate of one 0.5° step per drum every 150 sec after an initial delay of 50 sec. Whenever the controller receives a high-temperature signal, control drum rotation stops.

The temperature detectors utilized in the system are platinum resistance thermometers installed in thermowells located in the reactor outlet coolant line. Two temperature detectors are provided in the system. Each detector is the sensitive arm of a three-wire resistance bridge circuit with an adjustable null point. The output of the bridge circuit is amplified by a magnetic amplifier to drive an output relay. The bridge circuit, exclusive of the detector, the amplifier, and the output relay, constitutes the temperature switch assembly. The output relay contacts of the temperature switches are connected in series so that when both contacts are closed a high-temperature signal is developed at the controller input. If either contact opens, a low-temperature input condition exists.

The resistance-temperature characteristics of platinum are well-known and repeatable if the platinum is maintained strain free and in a pure condition. However, when assembled into a resistance thermometer, installed in a thermowell, and operated in a practical bridge circuit with a significant length of lead wire and high-temperature connections, a more complex relationship exists between the resistance of the detector and system temperature.

In the S10FS-3 system thermal reference test, the reactor control temperature detectors were connected in a special test bridge circuit designed to subject the detectors to measuring currents and voltages identical to those employed in the temperature switch circuits. This special test bridge provided sufficient resolution to accurately determine the relationship between detector resistance and system temperature. Calibration data were obtained at 600, 800 and 866°F with the system maintained at constant temperature for sufficient time to eliminate rate errors. The results of this system calibration are shown in Figure 1.

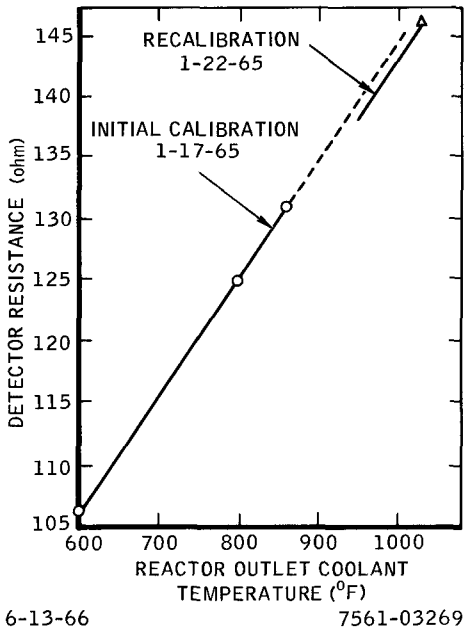

Figure 1. Reactor Control Temperature Detector Calibration Curves

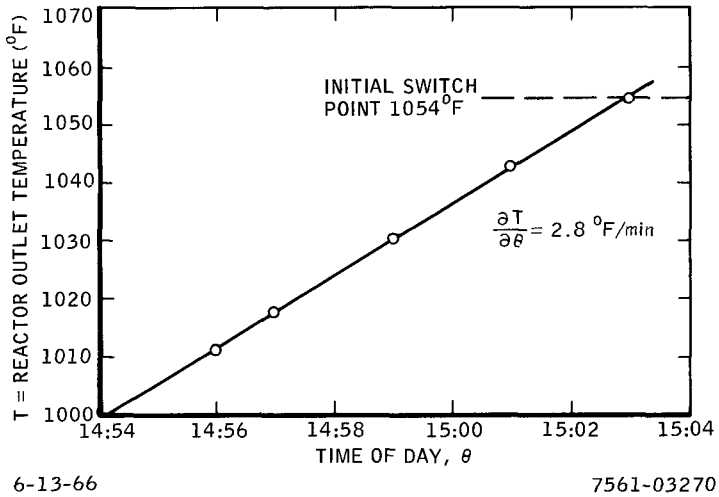

Figure 2. Reactor Outlet Temperature at Initial Switch Closure

The temperature switches were adjusted on the basis of the extrapolated initial calibration data to switch at 1010°F. Previous experience indicated that the installed detector had a thermal time lag of approximately 7 min. Therefore, with a system heat-up rate of 3°F/min expected as the reactor outlet temperature approached the set point, an overshoot of about 21°F above 1010°F was predicted for initial temperature switch closure on startup.

During the startup period, performance of the control system was as expected with the exception of temperature overshoot and temperature switch set-point control. When the startup controller was energized with the low-temperature condition existent, the controller initiated the control drum insertion at the rate of 1 step every 150 sec following an initial 50-sec delay. The reactor became critical, developed sensible heat, and raised the reactor coolant output temperature. As the temperature switch set point was approached, the reactor outlet temperature experienced a constant rate of change in temperature of approximately 2.8°F/min (Figure 2.) Switch operation did not occur at 1031°F as predicted, and the controller continued to operate until a temperature of 1054°F was reached, at which point switch actuation occurred. A check of the temperature switch set point

indicated that no changes were experienced by the switches. Measurements of detector resistances were made with the reactor outlet temperature near 1040°F. The results of this recalibration (Figure 1) indicate that the temperature detector resistance at a given temperature near the switch point was approximately 1.5 ohms less than that indicated from the initial calibration curve for the given temperature. With a detector sensitivity of approximately 0.0925 ohms/°F at the switch point, a decrease in detector resistance of 1.5 ohms results in a 16°F increase in switch set point. This observed change in detector resistance compares quite well with the 23°F difference deduced from the initial switch closure temperature.

The downward shift in detector resistance from the calibration curve is attributed to a change in the heat transfer characteristics between the detector and the detector-thermowell resulting from evacuation of air from the thermowell. The loss of the conduction and convective heat transfer by air in the well does not occur until the air pressure is significantly reduced. Since the air leakage is at a low rate, sufficient air remained in the well during the thermal reference test to provide good heat transfer between the detector and thermowell. Increasing the temperature above 866°F and additional time probably resulted in eventual loss of air, reduction in heat transfer capability, and consequently increased the difference between detector and fluid temperature. Subsequent tests on detectors in evacuated and unevacuated thermowells produced similar apparent changes in detector resistance.

The only components of the reactor control system installed within the vacuum vessel that were active in the FS-3 system test were the temperature detectors and actuators. The temperature switches and controller were located outside the vault. Wiring difficulties prevented obtaining any data from the instrument compartment controller and temperature switches installed in the FS-3 system.

The controller output period was correct about 93% of the time during startup. Significantly different time delay periods from the nominal 150-sec period sometimes occurred. Inspection of recorder data showed that incorrect time delay periods could be correlated with the occurrence of excessive noise on the system each time an incorrect delay occurred. Previous testing had shown that the controller was susceptible to electromagnetic interference. The excessive length of the system wiring in the FS-3 facility and added complexity of test system wiring (compared to the flight system) resulted in increased susceptibility of the controller to noise.

B. NUCLEAR PERFORMANCE

SNAP 10A predicted performance during reactor startup was based on prior analysis and on the experimental results obtained during dry and wet critical checks and during thermal reference tests. Electric heaters on the coolant inlet lines were used to isothermally increase the reactor temperature during the thermal reference test and the reactivity insertions required to maintain criticality during isothermal heating were measured. The reactor power was held constant at about 0.1 watt during the thermal reference test. Results of the dry critical, wet critical, and thermal reference tests for S10FS-3 are shown in Table 1.

TABLE 1

RESULTS OF DRY AND WET CRITICAL CHECKS AND STARTUP LOSSES FOR S10FS-3

	S10FS-3 (1 shim) ($)
Excess reactivity at cold, dry critical	2.64
Excess reactivity at cold, wet critical	2.95
Isothermal temperature defect 80 to 1010°F	2.12
Reactivity inserted to reach full power	1.92
Excess reactivity at full power	1.02
Reactivity inserted (control drums) during active control period	0.49
Excess reactivity at end of active control period	0.53

Prior to the automatic startup of S10FS-3, it was expected to require 8.5 hr from the time of the startup command to the achievement of full power. The position of the fine control drums at full power was expected to be 30.3° from full in and the temperature and power defect was expected to be $2.13. During the actual automatic startup, full power was attained in 8.0 hr with the drums at 33.7° from full in. The discrepancy between these values and those predicted is due to the lower than predicted value of the temperature and power defect ($1.92). The reactor outlet temperature and drum position for S10FS-3 during startup are shown in Figure 3. As discussed in Appendix A, the reflector mounting was

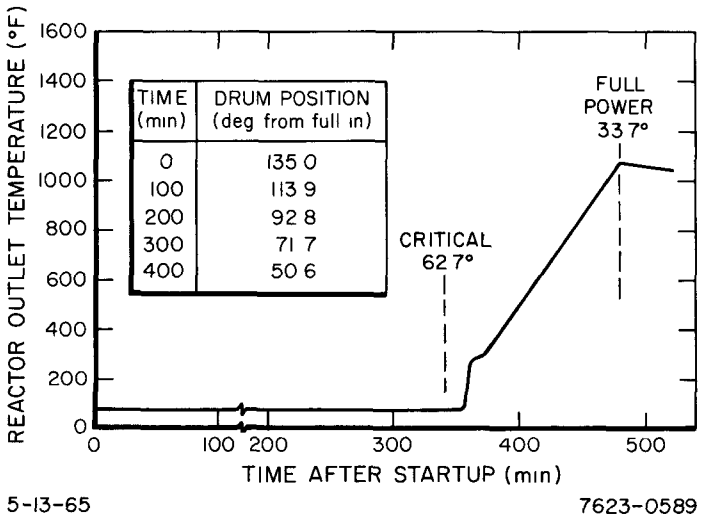

Figure 3. S10FS-3 Reactor Performance During Startup Period

modified to allow remote removal of the reflector. This allowed the reflector to be moved abnormally by frictional forces during periods of differential expansion. During the period when the reactor temperature was increasing, it was estimated that a maximum of 11¢ per reflector half could be inserted by horizontal inward motion of the bottom of the reflector halves. Since the -Z reflector half returned to its seated position 17 hr after startup, it was judged that only a 4 or 5¢ insertion was associated with movement of this half. An estimated total of 16± 4¢ of reactivity was added by movement of the reflector during startup.

If the preceding estimate for reactivity inserted by reflector movement is added to the reactivity inserted by control drum insertion, the temperature and power defect is calculated to be $2 08± 0.04 This is in much better agreement with the predicted defect of $2.13.

Based on these observations and using the predicted NaK temperature prior to reaching sensible heat, predictions of S10FS-4 startup performance were made.[1,2]

C THERMAL AND HYDRAULIC PERFORMANCE

Power and temperature transients observed during the initial penetration into the power range generally confirmed the appropriateness of the mathematical model used in predicting S10FS-3 startup performance. Some modifications of this model were made, however, on the basis of the startup data. The major correction necessary in the thermal model of the reactor was the

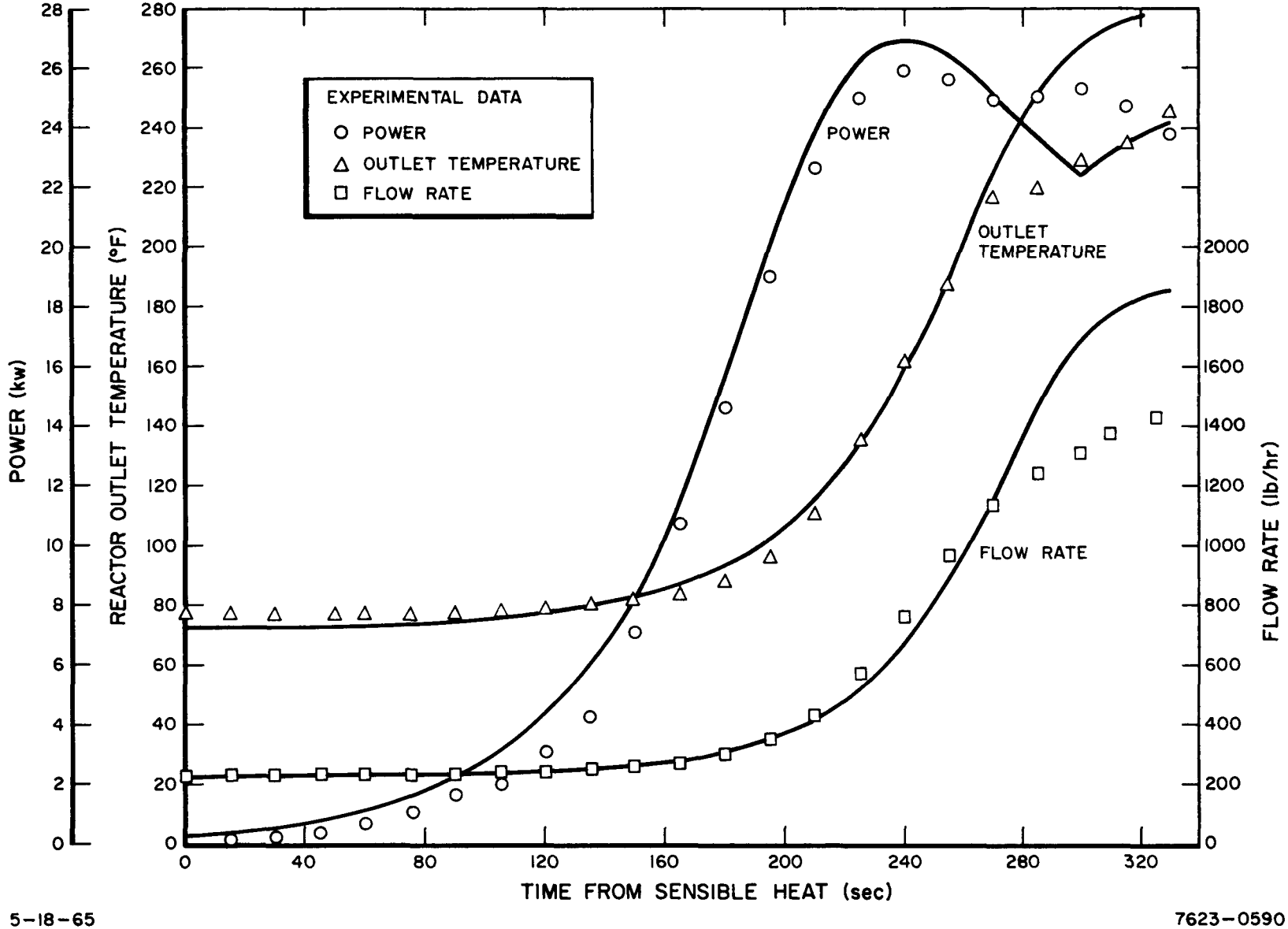

5-18-65

7623-0590

Figure 4. Comparison of Calculated and Observed Startup Transients

inclusion of the beryllium internal reflectors which contribute significantly to the total reactor heat capacity. It was also necessary to make minor modifications in the thermal model to account for the actual location of the reactor inlet and outlet thermocouples at positions upstream and downstream, respectively, from the physical core inlet and outlet. The value of the overall heat transfer coefficient, UA, calculated for the low-temperature range (0.70 to 0.85 kw/°F) yielded results which agreed well with the observed startup performance. The coefficient is definitely much larger than the 0.15 to 0.20 kw/°F experimentally determined on the S2DR reactor (at 800 - 900°F).

The changes made in the reactor model include:

1) the design-nominal 0.5° drum stepping angle used in all previous analyses was increased to the observed value of 0.528°,

2) the absolute value of the negative fuel temperature coefficient was increased slightly over the S2DR experimental values (-0.107¢/°F vs the S2DR derived value of -0.092 ¢/°F at 300°F), and

3) the actual drum step times were programmed into the analyses.

The FS-3 initial startup transient generated by the revised model is compared to the actual test data in Figure 4.[3] The analysis assumes a multiplied source strength of 5.58×10^{-7} kw. The predicted peak power is 26.9 kw as compared to the actual 25.9 kw, a difference of 3.9%. The 20-sec difference in the timing of the drum step following peak power (300 sec vs 280 sec) is probably due to a small error in the reactor shutdown worth. Reactor outlet temperature matches the experimental data well until about 260 sec past sensible heat. Then, for a short time, the calculated temperature increases more rapidly than does the data. The reason for this discrepancy is not known. The calculated and experimental curves do converge as the power continues to decrease. The flow rate follows the reactor outlet temperature in an identical manner for both transients.

An examination of the core thermal transient from sensible heat through 340 sec subsequent to sensible heat revealed no calculated condition where excessive thermal stresses could have occurred within the reactor core during this period (which includes the most severe transients experienced during startup). Discontinuity stresses at the junction of the upper end cap and cladding on a fuel element are caused by the differential expansion between the upper end cap and the adjacent cylindrical cladding. The maximum stresses

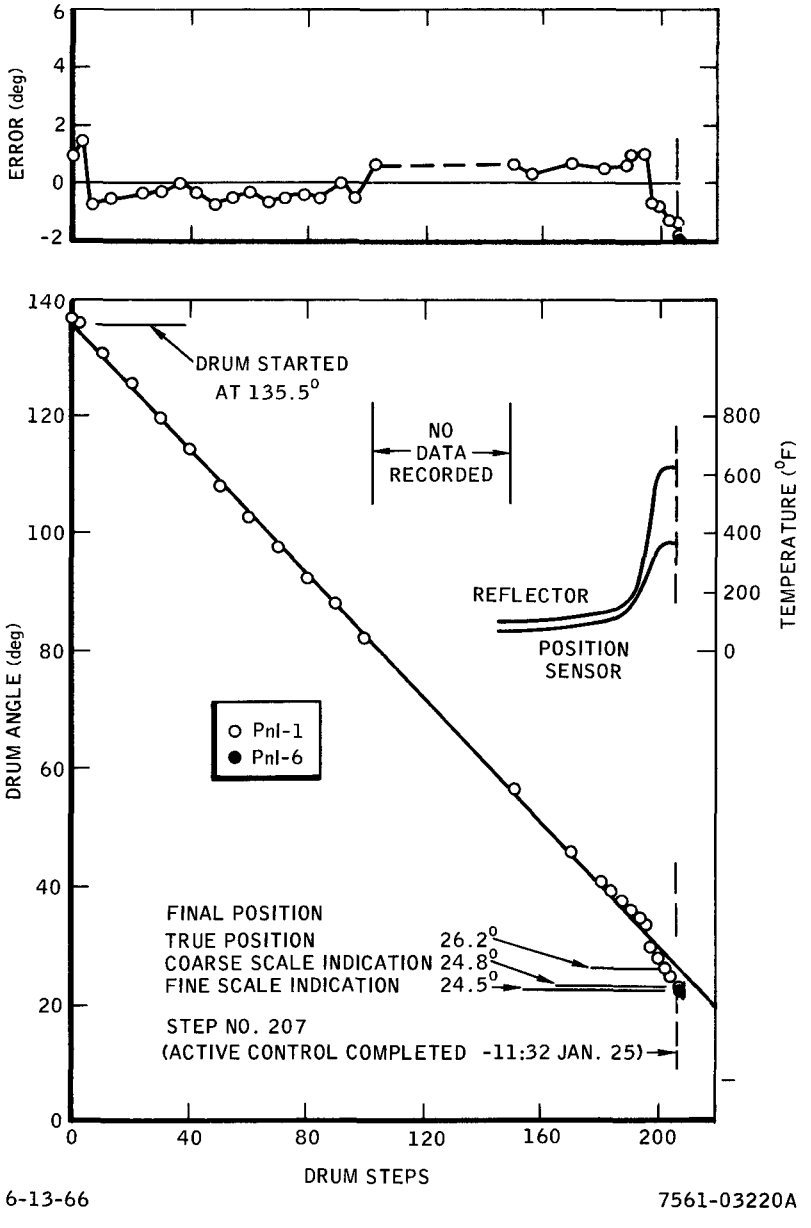

Figure 5. Performance of Coarse and Fine Control Drum No. 3 Position Sensors

calculated for the center fuel element, were ± 16,000 psi in the cladding and ± 5320 psi in the barrier. Because the barrier has a residual precompression stress of 25,000 psi, it remains in compression throughout startup. The calculated maximum stress within a fuel rod was only 800 psi.

D. DIAGNOSTIC SYSTEM PERFORMANCE

1. Limit Switches

All control drum limit switches and the reflector retaining band limit switches operated as expected.

The reflector position indicating limit switches, PnS-15 and PnS-16, gave indications of "Reflector-off" shortly after the start of the reactor heatup ramp. It has been rationally argued that these switches were actuated by upward movement of the reflector assembly relative to the reactor vessel rather than by switch malfunction or movement of the switches relative to the reflector assembly. An evaluation of the FS-3 reflector installation which describes this movement is reported in Appendix A.

2. Control Drum Position Indicating System

Voltage output from the control drum position sensor demodulators was recorded at 15-min intervals during the FS-3 startup. Because the control drums did not start from the locked-out position, it was necessary to establish the true drum starting position before the performance of the control drum position indicating system could be fully evaluated. This was accomplished by a detailed study of the position indicating system output data which were then correlated with the known nuclear data for the drums. It was established that the No. 3 drum (+Z) started at 135.5° from full in and the No. 4 drum (-Z) started at 133.0° from full in. It was also established that the drum consistently moved when power was applied to the actuators.

Knowing the true drum starting position and the drum rotation angle per actuator step (0.528°), a graph was drawn of true drum position vs motor steps. The indicated position, established by the sensor-demodulator calibration curves and the recorded output voltages, was compared with the graph.

The indicated position of drum No. 3 (+Z) is shown in Figure 5 relative to the established true drum position. Except for the starting position, the

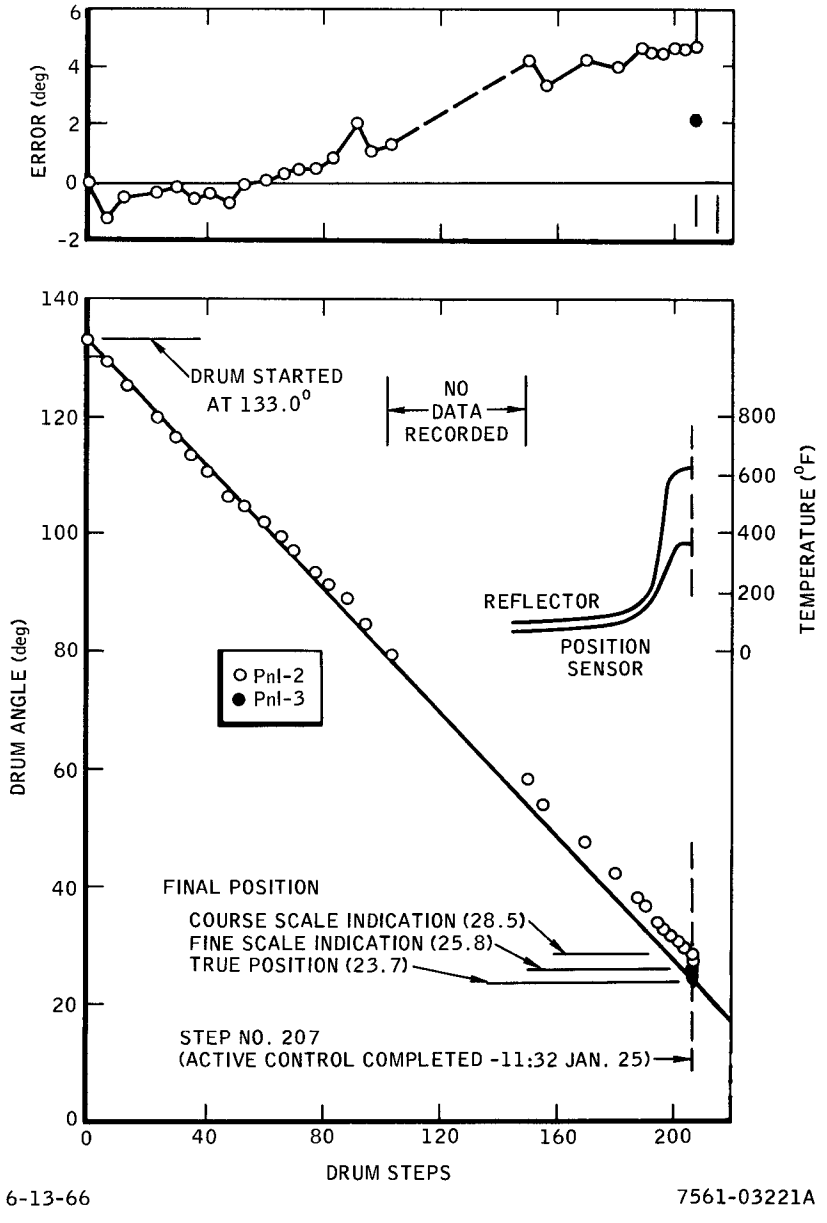

Figure 6. Performance of Coarse and Fine Control Drum No. 4 Position Sensors

position after the first step and last few steps before reaching full power, the deviations are less than 0.5°. There is no explanation for the erratic nature of the first two readings which show deviations of +1 and +1.5°, respectively. As the drum approached the full power position (Step 192), the deviation increased slowly and reached approximately 0.75° at Step 192.

Figure 6 shows the indicated position of drum No. 4 (-Z) relative to true drum position. The deviation was small, generally about 0.5° low over the first 30° of drum rotation. At approximately 30° "in" the slope of output vs angle changed so that the deviation increased linearly throughout the remainder of the control period and was 4.5° high at Step 192.

The change in the slope of output vs angle that occurred on the drum No. 4 position indicator does not correlate with reflector temperature change or any other known factors. The direction of the change coincides with a downward movement of the rotor shaft. The shaft movement must have been gradual with drum angle or an offset in the calibration curve would have occurred.

The sensor calibration is not affected by a downward force on the shaft starting from a zero-load condition because the sensor has an internal spring which loads the rotor shaft downward against the rear thrust bearing. If shaft movement were the cause of the deviation in the drum No. 4 indicated position, it would have had to occur as an initial upward deflection which remained constant over the first 30° and then moved downward.

BLANK

IV. ACTIVE CONTROL PERIOD

A. CONTROL SYSTEM PERFORMANCE

During the active control period the controller was expected to step the drums inward whenever either temperature switch was open. The first step occurs 50 sec after switch opening and subsequent steps occur every 150 sec thereafter. Upon switch closure the controller immediately resets itself to the 50 sec count. It was predicted that, after taking the first step, the temperature switches would close before 150 sec had elapsed so that only one step would be taken each time the switches opened. The temperature switches were expected to switch closer to their nominal set points as the ramp rates became less and the effect of time constant was decreased.

During the active control period, with one exception, the controller took two steps each time the switches opened. A total of 15 steps was taken subsequent to the initial switch closure. The switch openings occurred as shown in Table 2.

TABLE 2
S10FS-3 TEMPERATURE SWITCH ACTUATION

Time	Outlet Coolant Temperature at Opening (°F)	No. of Steps	Maximum Outlet Coolant Temperature after Stepping (°F)
1545 - 1/22/65	1023	2	1062
1634 - 1/22/65	1028	2	1070
		Switches Readjusted	
1906 - 1/22/65	1008	2	1051
2313 - 1/22/65	1008	2	1053
0608 - 1/23/65	1008	1	-
1102 - 1/23/65	1007	2	1047
0056 - 1/24/65	1007	2	-
1115 - 1/25/65	1007	2	1049
1500 - 1/25/65	Controller Off		

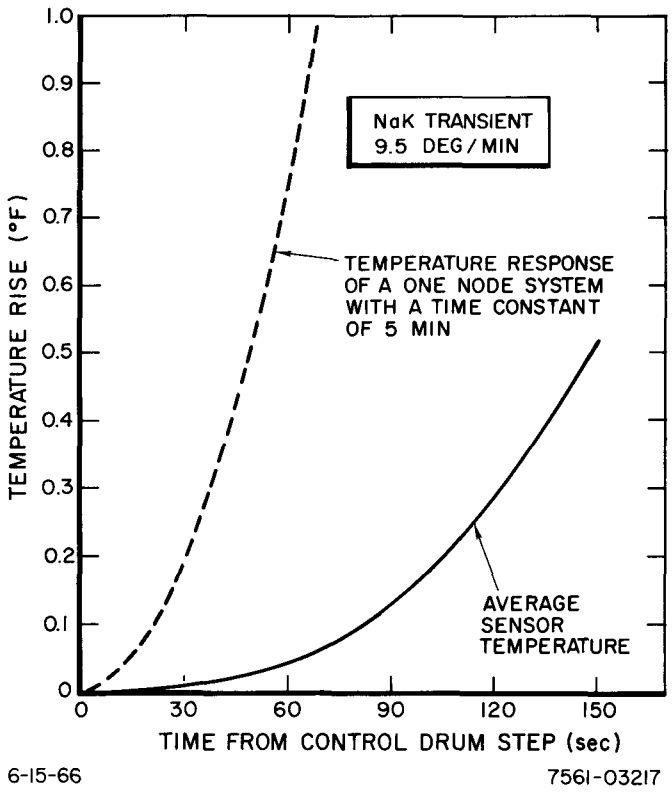

Figure 7. Sensor Element Temperature Response

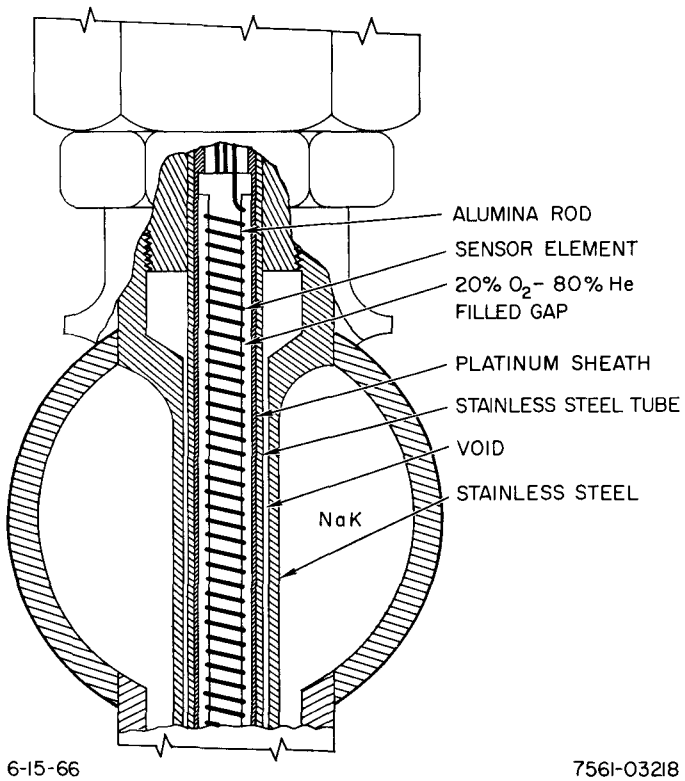

Figure 8. SNAP 10A Temperature Sensor Element

As seen in the table, the set point was about 1028°F, the switch opening temperature with a slow ramp rate, before readjustment. This is 18°F above the expected set point and is in good agreement with the 16 to 23°F difference deduced in Section III. A. After readjustment the set point was about 1007°F.

During this 72 hr period the controller took one abnormal delay period of approximately 80 sec subsequent to the 2313 1/22/65 switch opening. This abnormal delay period has been attributed to a random noise pulse in the facility electrical system.

The response of the temperature detectors has been analyzed to obtain an explanation of the controller allowing two control drum steps per switch opening. Hysteresis of temperature switches (difference between pull-in and drop-out) is 0.05 ± 0.01 ohm (0.5 ± 0.1°F), as shown from the pre- and post-acceptance level vibration measurements on 21 switches. On the 2 switches used in FS-3, S/N 1008 and 1013, the hysteresis was 0.04 and 0.05 ohm (0.4 and 0.5°F), respectively. To explain the double steps, the average detector temperature rise during the 150 sec period following a drum step must be less than this hysteresis.

The response of the detector assembly was calculated assuming a 5 min time constant, later shown to be somewhat low, though not enough to invalidate the results of this analysis. It was found that the temperature of a one-node mathematical model with this time constant would increase an amount equal to the hysteresis within 50 sec, as shown by the dashed line in Figure 7. A detailed mathematical model of the detector was constructed to permit evaluation of the effect of axial temperature distribution in the detector element. The heat flow from the NaK to the detector element (Figure 8) is by parallel high resistance paths. These are: 1) conduction along the stainless steel wall tube with radiation to the inner tube and subsequent radiation to the element, and 2) conduction to the detector head and into the alumina rod. The relatively high resistance to heat flow by radiation across two gaps or conduction in the alumina inner rod results in a significant amount of heat being conducted into the detector head and connectors during transient heating. The detailed mathematical model yielded startup transients in good agreement with FS-3 data and shows (Figure 7) that the time following a drum step for the average detector temperature to increase an amount equal to the hysteresis was about 150 sec. This explained how a second step could be taken prior to the temperature switch closure.

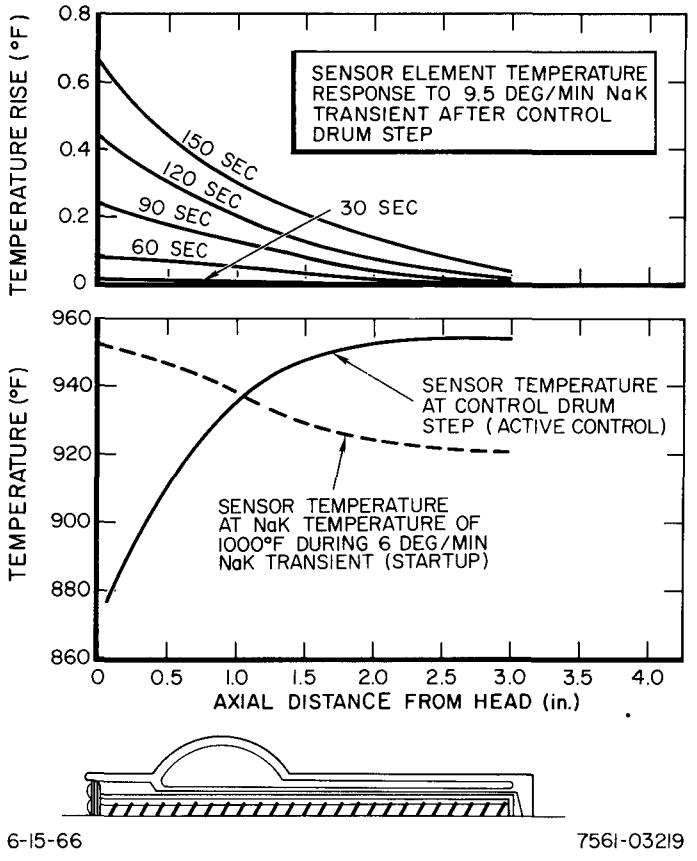

Figure 9. Sensor Element Temperature Profile

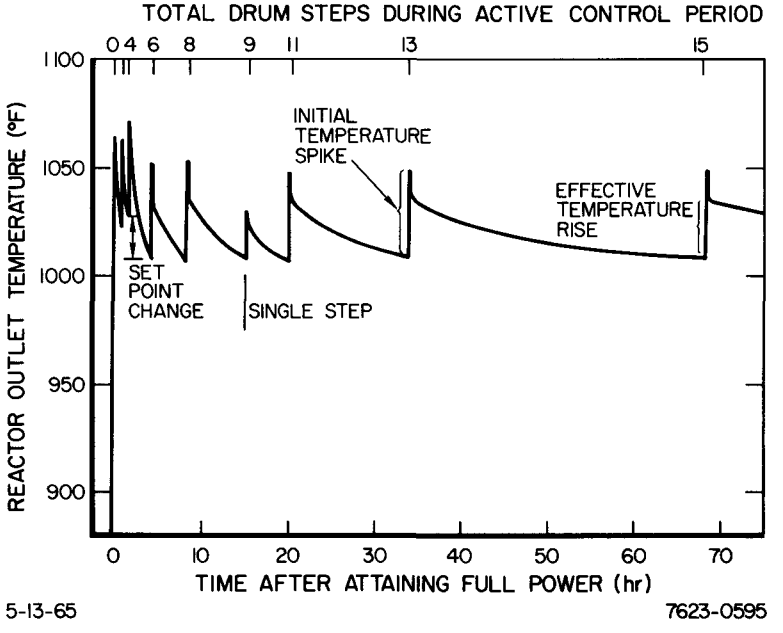

Figure 10. Reactor Performance During Active Control Period

Figure 9 explains a reason for the slow initial response. In the lower half of the figure the detector axial temperature profiles are shown for the startup transient and steady-state (before drum step) cases. In the upper-half is shown the temperature rise along the detector for different times following a drum step. The slow initial response in detector average temperature is due to the slow temperature increase at points far from the detector head as the startup transient profile is being re-established.

B. REACTOR PERFORMANCE

Temperature behavior of S10FS-3 during the active control period is shown in Figure 10. The temperature rise after each reactivity insertion is determined by the size of the reactivity insertion and the prompt temperature coefficient of reactivity. The prompt reactor temperature coefficient for S10FS-3 was determined, from response to the step reactivity insertion, to be -0.13 ± 0.02¢/°F. The prompt temperature coefficient is attributable to combined prompt fuel and upper gridplate coefficients. Analysis of the reactivity coefficients after temperature, power, and power dependent effects have stabilized indicates that the final effective temperature coefficient is -0.29 ± 0.02¢/°F, in good agreement with data from the isothermal tests.

The most significant reactivity losses which occur during the SNAP 10A 72 hr active control period are; 1) xenon buildup to saturation, 2) reflector heating to equilibrium temperature, and 3) hydrogen redistribution. In addition to these effects, reflector slippage was an important loss contributor in FS-3. Reactivity losses due to fission product accumulation, U^{235} burnout, and hydrogen loss are essentially compensated by Sm^{149} prepoison burnout. The net loss due to these "long term" effects is essentially negligible during the short active control period.

The predicted contributing reactivity losses are compared to losses deduced from the observed reactor performance in Table 3.

The observed total reactivity loss during active control is compared to the predicted loss in Figure 11. Figure 12 illustrates the deduced contributing reactivity loss effects. It is noted that the experimentally observed loss was

TABLE 3

PREDICTED AND OBSERVED REACTIVITY LOSSES DURING S10FS-3 ACTIVE CONTROL PERIOD DURING FIRST 68 HOURS AT FULL POWER

	Predicted (¢)	Deduced From Observed Performance (¢)
Reflector Defect*	14.7	14.7 ± 0.7
Xenon Buildup	17.2	20.0 ± 2.0
Hydrogen Redistribution	11.1	3. ± 2.0
Abnormal Reflector Movement	-	11. ± 2.0
Total:	43.0	48.7¢ ± 4.2¢

*Prediction corrected to observed reflector temperature

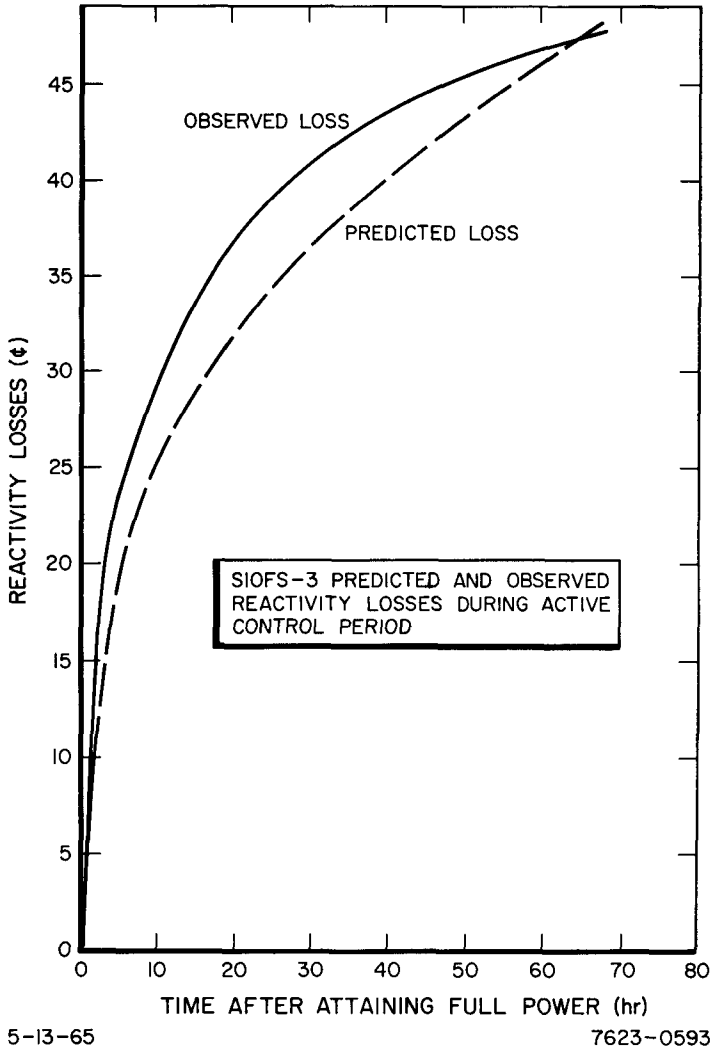

Figure 11. Predicted and Observed Reactivity Loss During Active Control Period

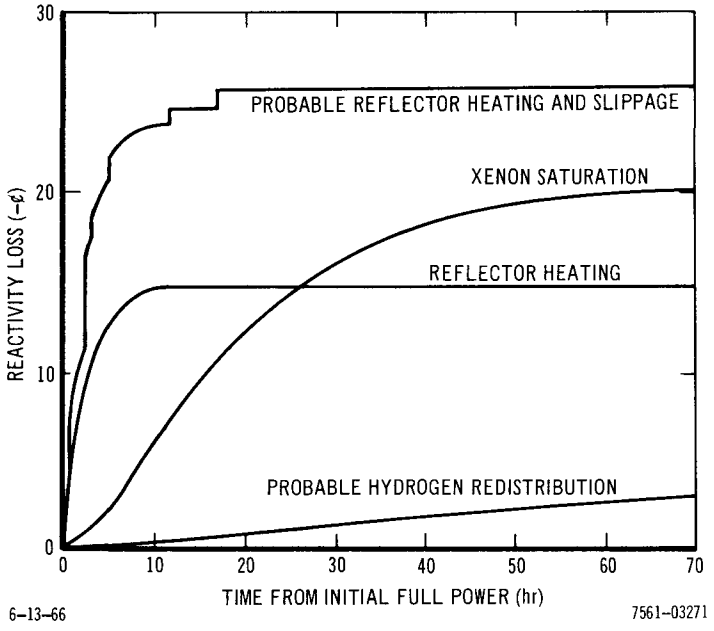

Figure 12. S10FS-3 Active Control Period Reactivity Losses (Deduced From Observed Total Loss)

initially at an appreciably faster rate than predicted but that the reactivity loss rate became considerably less than predicted at about 30 hr after attaining full power (Figure 11). Several factors are believed to have contributed to the deviation from the prediction. These factors are discussed in the following paragraphs.

1. Reflector Defect

The reflector defect is the result of reflector heating (by radiation from the reactor vessel and by internal heat generation) which occurs over the first 15 hr of the active control period. Heating causes the reflector to expand and move away from the reactor vessel and also reduces the beryllium density. Both effects result in reactivity loss.

2. Xenon Buildup to Saturation

Average reactor power during the active control period was about 42 kw. Since xenon equilibrium worth is nearly proportional to power in the relatively low-flux SNAP 10A reactors, the 17.2¢ prediction for 37 kw was adjusted to 20¢ to account for the change from predicted power.

[redacted]

3. Hydrogen Redistribution

Zirconium hydride is an intermetallic compound in which the hydrogen ions tend to migrate to the colder portions of the material due to thermal diffusion. The hottest region of a reactor fuel rod is the highest neutron flux region. The hydrogen worth is approximately proportional to the square of the neutron flux, so that the hydrogen migration effectively results in a reactivity loss.

The hydrogen redistribution contribution to the S10FS-3 active control period reactivity loss was significantly less than predicted. The effect deduced from the experimental data indicates that only about 3¢ of hydrogen redistribution occurred during the active control period. This is considerably less than the predicted 11.1¢ hydrogen redistribution for the active control period.

The total operational S10FS-3 hydrogen redistribution effect was calculated to be 22¢ ± 6¢. The 90 hr time constant for hydrogen redistribution, previously calculated with the HYTRAN[4] computer code, indicated that 11.1¢ of the total effect would occur during the active control period. A logic error in the HYTRAN model was subsequently discovered and corrected. The model now predicts a 3000 hr time constant for FS-3 nominal operating conditions; but it is not accurate during the first few hundred hours of operation. The (about 3¢) hydrogen redistribution effect deduced from active control period data is not in disagreement with the calculated effect. HYTRAN indicates an initial small positive redistribution effect of a few hours duration, followed by negative redistribution with a time constant shorter than the calculated equilibrium value. Qualitatively, these results appear to be correct; however, the magnitude of the effects which occur shortly after attaining full power are acknowledged to be in error due to oversimplification of the model (e.g., neglecting axial hydrogen redistribution between fuel element nodes).

Due to the large uncertainty in the reflector motion effect, and in the redistribution analysis during the initial period of operation, an uncertainty of ± 2¢ must be assigned to each of these effects. The uncertainty of the combined effects is about ± 3¢.

[redacted]

4. Reflector Movement

Reflector motion is discussed in some detail in Appendix A of this report. Figure 12 shows the magnitude of the reactivity effect implied from the observed active control period data. Reflector movement is indicated at the times of control drum motion because those are the most probable times of occurrence (as indicated by a test, Appendix A) and because no sudden temperature changes were observed at any other time during the active control period.

Using the reactivity loss rate data from S10FS-3, and correcting for abnormal reflector movement and the expected higher reflector temperature in space, a prediction of reactivity losses during the S10FS-4 active control period was made[1,2].

C. COMPONENT TEMPERATURES

1. Reflector

The S10FS-3 reflector temperatures are shown in Figure 13 for the stabilization period. These temperatures were at their steady-state values of about 620°F within 18 hr after the time of sensible heat. The analytical curve shown in Figure 13, which agrees closely with the measured temperatures, was determined using an emissivity of 0.4 for the bare beryllium surfaces on the reflector. This analytical curve stabilizes at 630°F.

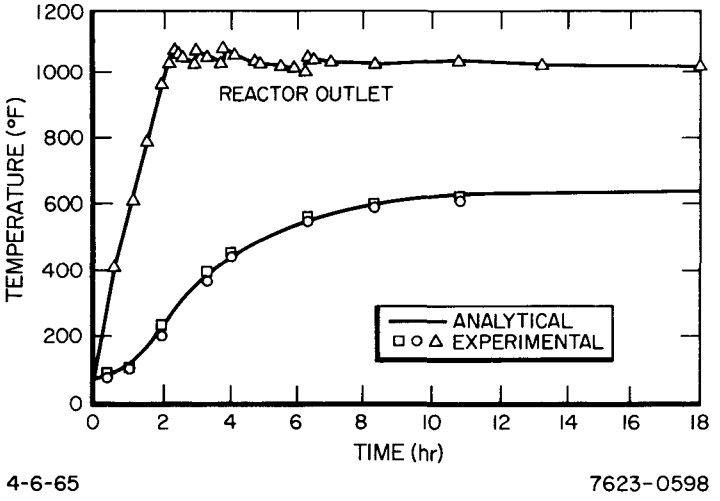

Figure 13. Comparison of Calculated and Measured Reflector Temperatures

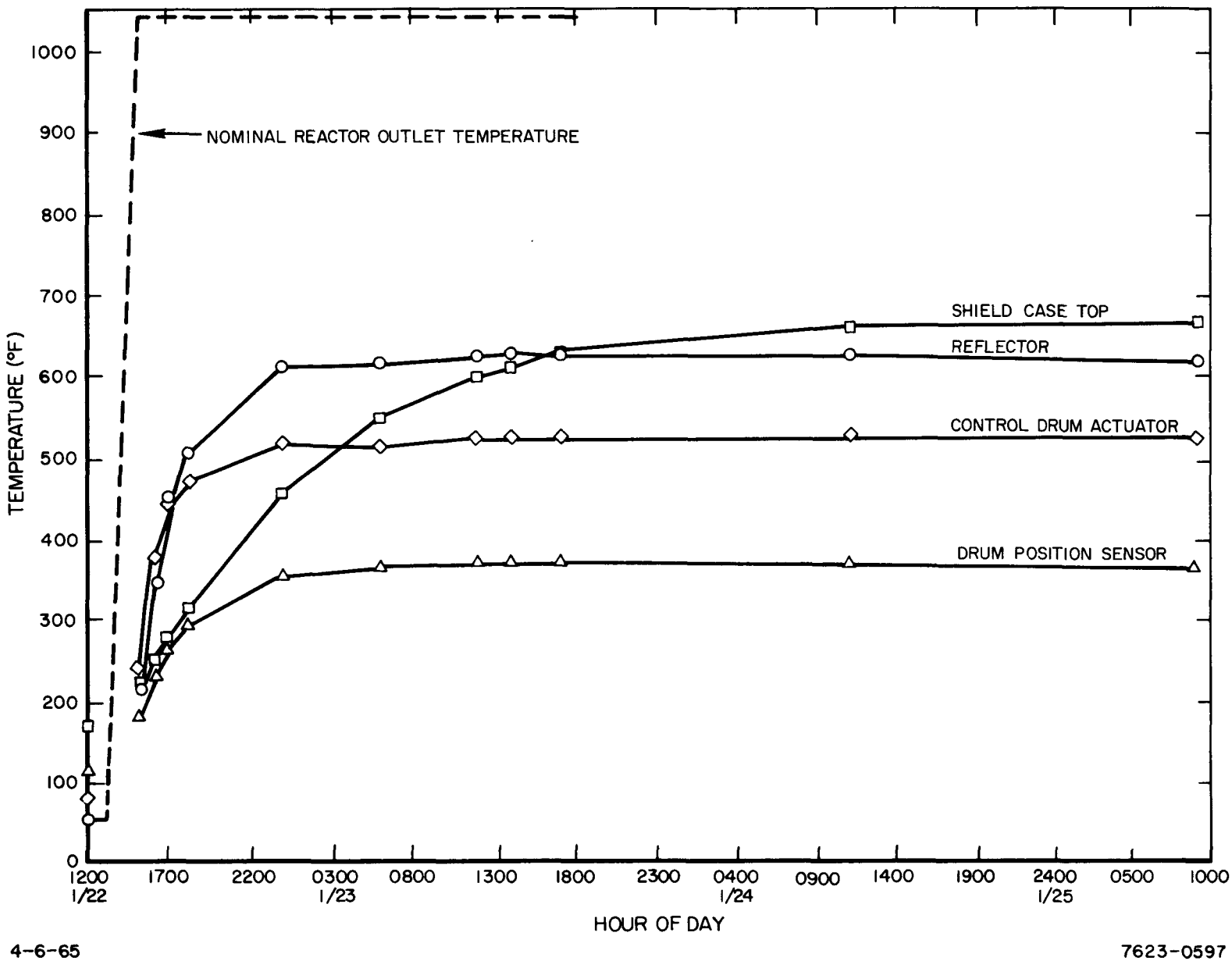

Figure 14. Measured Component Temperature Transients

2. Radiation Shield

The predicted steady-state temperature at the top of the SNAP 10A shield casing was 680°F. The calculated internal shield temperature below this point was 670°F. The maximum computed temperatures in the shield and the casing were about 805°F and occurred near the bottom of the shield.

Figure 14 shows the observed temperature transient for a thermocouple located near the top of the FS-3 shield case. The steady-state reading of this thermocouple was 675°F. The calculated shield casing temperature at the radial location of the thermocouple was about 640°F. The difference between the calculated and observed values is caused by a NaK coolant pipe in the proximity of the thermocouple so that the casing temperature at this location is above the circumferential average obtained in the analysis.

Internal shield thermocouples malfunctioned during the S10FS-3 test, so that only shield casing data were available for comparison with predictions.

3. Drum Actuators and Position Sensors

Figure 14 shows temperature transients for an inboard thermocouple on one of the control drum actuators and for a position sensor thermocouple. The inboard actuator thermocouple attained a steady-state temperature of 530°F. (A thermocouple mounted on the outboard side of the actuator reached 510°F.) The position sensor thermocouple plotted in Figure 14 reached a temperature of 370°F; another thermocouple installed in an equivalent location read 340°F.

No detailed analyses had been performed to predict the temperatures of these components. Instead, limiting-case studies had been made to determine upper limits of operating temperatures for the purpose of establishing qualification criteria for these components. These upper limits were 700°F for the actuators and 500°F for the position sensors. The observed operating temperatures were well below these limits.

D. DIAGNOSTIC SYSTEM PERFORMANCE

1. Limit Switches

Approximately 14 hr after reaching full power, +Z reflector ON-OFF limit switch, PnS-15, opened and thereby corrected the indication of reflector

ejection that was first noted during the startup phase. The later opening of the switch is attributed to the downward expansion of the reflector as it came to temperature or to slippage between the reflector top adjusting bolts and the reflector upper stop surfaces.

The reflector OFF indication of PnS-16 (the -Z reflector ON-OFF limit switch) remained throughout the active control period. The status of all other limit switches remained normal during this period.

2. Control Drum Position Indicating System

The calibration and sensitivity of PnI-1, the +Z control drum position indicator (coarse scale), shifted between 1-1/2 and 4 hr after the reactor reached full power. The shift is shown in Figure 5. The shift in calibration was approximately 1.5°, from 0.75° high to 0.75° low, and the change in sensitivity was from 31 to 41 mv/degree. The change occurred in two increments, the first 0.5° shift at step No. 195 (1-1/2 hr after reaching full power) and the remaining 1.0° at step No. 197, 2-1/2 hr later. Due to the change in sensitivity, the deviation increased from 0.75° low to 1.5° low as the drum was rotated through steps No. 198 through No. 207, where active control was stopped. The deviation between indicated and true drum position for PnI-6, the No. 3 drum fine scale, was 1.7° low at the end of the active control period.

The shift in the indicated position of drum No. 3 took place during the time the reflector temperature was increasing. The direction of the shift and the subsequent change in slope coincide with the effect of the exertion of an upward force upon the sensor shaft. The upward force reacts against the sensor bearing preload spring and moves the rotor.

Normally, an upward force on the sensor shaft is prevented by preloading the sensor shaft in a downward direction with a 500-gram load by installing the flexible coupling so that it is extended 0.010 in. from its free position. On FS-3 the preload was inadvertently omitted when the sensors were reinstalled after being removed to install the shear pin through the coupling and the sensor shaft.

PnI-2, the No. 4 drum control drum position indicator (coarse scale), did not change in calibration or sensitivity (Figure 6) during the active control period. At initial full power the deviation was 4.5° high and increasing. The

deviation increased at the same rate to 4.8° at the end of active control. The deviation between indicated and true drum position for PnI-3, the No. 4 drum fine scale, was approximately 2.1° high at the end of the active control period.

BLANK

V. ENDURANCE PERIOD

A. REACTOR PERFORMANCE

The control system was deenergized with the average NaK temperature at 973°F on January 25 after 72 hr of active control. During the initial week of statically controlled operation, reactor behavior was very similar to that previously predicted. Approximately two weeks after cessation of active control, the average coolant temperature was above the nominally predicted value, adjusted to the initial value of 973°F, but was decreasing at a higher rate than predicted. This performance is shown in comparison to the pretest predictions in Figure 15. This figure shows the predicted positive long-term temperature drift and predicted year-end temperature of $944\ ^{+42}_{-39}$ °F.

The observed long-term temperature drift was significantly greater than the nominal predicted drift. The minimum temperature was not, however, significantly different from the predicted minimum. Analysis of reactor performance was continued throughout the static control period and performance extrapolations were periodically made.

Upon completion of the full year of static control operation, daily average temperatures were obtained from the S10FS-3 data record tapes and were differentiated as shown in Figure 16. This figure shows that the temperature drift rate changed from negative to positive after 250 days of operation; and changed back to a negative rate after about 300 days. The nuclear models employed for analysis predict a smoothly decreasing negative temperature derivative for the 50-day period, as shown by the dashed line in Figure 16. It has been hypothesized that fuel swelling might have closed the fuel rod to cladding gap, resulting in a reduction in fuel temperature. Reducing the fuel temperature would effectively add reactivity and could result in the observed increase in reactor power level. Once the gap closing was complete in the affected elements, the temperature drift curve would return to the previous slope. The low burnup in SNAP-10A does not result in a significant amount of swelling. Therefore, swelling resulting from zirconium-hydride phase boundary movements is the only mechanism considered credible for causing the hypothesized gap closure. Because of the uncertainty in this hypothesis, the positive drift will continue to be referred to as "unexplained." Additional information may be gained from the post-test fuel element examination which is currently under way.

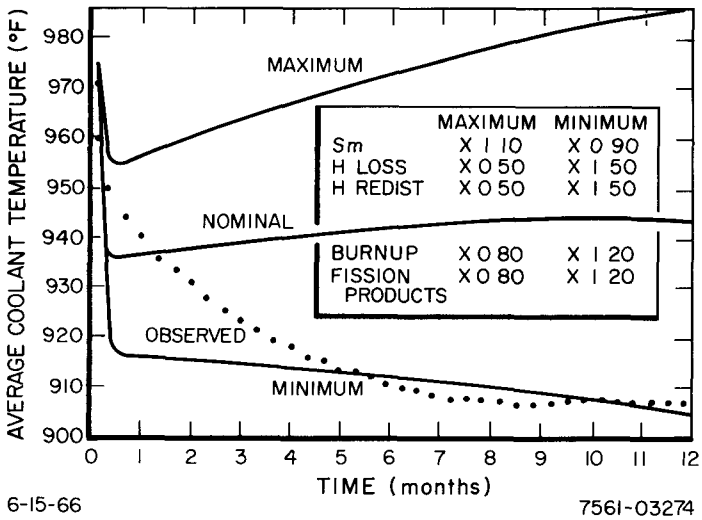

Figure 15. Predicted and Observed Static Control Period Performance

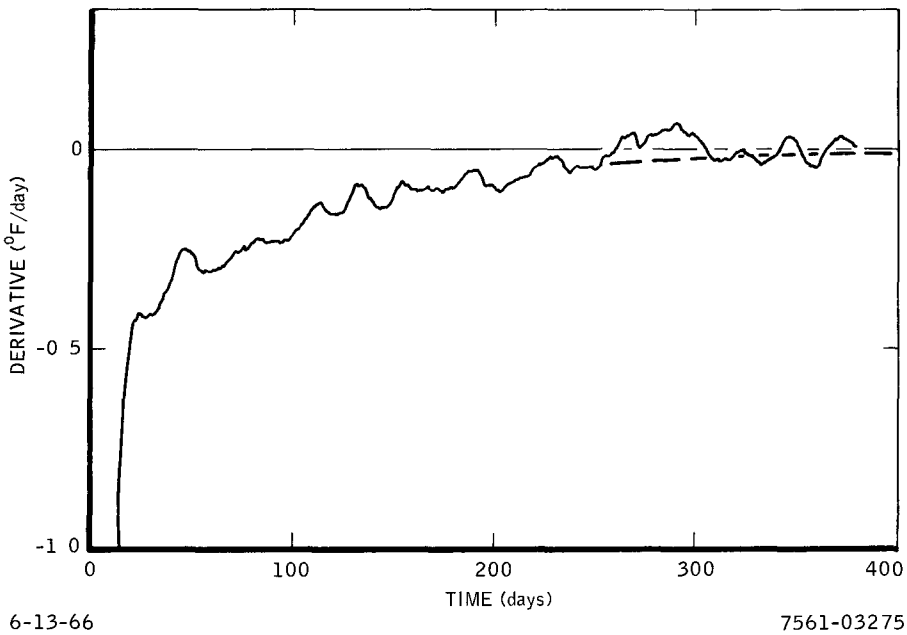

Figure 16. First Derivative of S10FS-3 Average Coolant Temperature During Static Control

The temperature derivative in Figure 16 also appears to be cyclical with a period of about one month. This cycling is apparently not a result of the smoothing routine. A review of the facility operating procedures and schedules has not revealed any correlatable events, and the nuclear analysis has disclosed no cyclical phenomenon.

Figure 17 shows the plotted daily average coolant temperature and the "unexplained" positive drift between 250 and 300 days. The net difference in year

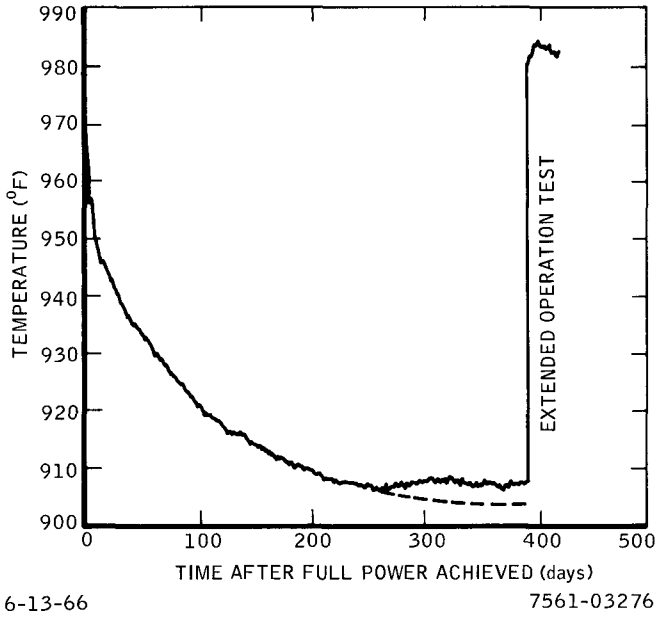

Figure 17. Static Control Performance With and Without Unexpected Drift-Up After 250 Days

end temperatures (between observed and smoothed) is about 3.5°F. The smoothed performance shown by the dashed line was based on performance up to 250 days, and on the smoothed temperature derivative of Figure 16. The year-end average coolant temperature indicated by this analysis was 903°F. This is interpreted as the year-end condition which would have existed if the unexplained positive temperature drift had not occurred.

A careful examination has been made of the data logger system which showed that the deviation in long-term drift from the original prediction (Figure 15) could not be attributed to any electronic problem, but was actually from reactivity loss mechanisms affecting the reactor. This was further verified by data from operation of the FS-4 system.[2]

All primary and secondary reactivity losses mechanisms have been reexamined using improved techniques and experimental data where available. This reevaluation has resulted in revised estimates for several reactivity effects and improved estimates of analytical uncertainties, and has helped pinpoint areas of uncertainty which require additional experimental examination. In this section, the original SNAP 10A performance predictions are first discussed for reference and then the reevaluation of the performance is discussed in detail.

Because of the importance of the endurance performance of FS-3 to static control reactor technology, a discussion of the extrapolation of each of the reactivity loss mechanisms to a higher temperature, higher powered reactor

is included in Appendix B. The important conclusion here is that static control is feasible at the higher operating conditions since the uncertainty in performance predictions would not be much larger than for a reactor operating at the current SNAP 10A conditions.

1. Original SNAP 10A Performance Predictions

The original analysis of SNAP 10A static control period reactivity losses had shown that the primary reactivity loss mechanisms were: 1) hydrogen redistribution, 2) hydrogen loss, and 3) fuel burnup and fission product accumulation. The reactivity losses were calculated using the best analytical techniques available. The samarium prepoison loading was then selected so that the reactivity gain due to prepoison burnout was greater than the calculated reactivity losses (Exclusing hydrogen redistribution).

Xenon, a rapidly saturating fission product, was calculated to be 95% saturated after 72 hr of full-power operation. The active control period was specified as 72 hr to allow automatic reactivity compensation for xenon and a portion (about one-half) of the hydrogen redistribution effect.

a. Hydrogen Redistribution

The hydrogen redistribution effect was calculated with the HYTRAN code (4). This computer code calculated the temperature distribution within a SNAP 10A fuel rod from the power density, coolant flow rate and thermal characteristics of the fuel element and coolant. The hydrogen distribution, both axially and radially, within the fuel rod was then calculated as a function of time using the accepted hydrogen diffusion coefficient and heat of transport. The reactivity loss was calculated using the experimentally determined worth of hydrogen in the SNAP 10A core. HYTRAN calculations indicated that the total 22 cents of hydrogen redistribution would be completed about 21 days after reaching full power with approximately 50% occurring after static control was initiated (with a 70 hr time constant). Uncertainty in the hydrogen diffusion coefficient and heat of transport in zirconium resulted in an estimated uncertainty of ±50% in the reactivity loss after 72 hr of operation. Experimental data from S2DR reactor operation indicated that the actual redistribution time constant might be considerably longer than the HYTRAN calculations shows.

b. Hydrogen Loss

Hydrogen loss was calculated with the HYLO computer code. Fuel temperatures were calculated at several nodes within the fuel rods to determine average fuel temperatures and, hence, average hydrogen gas pressure in fuel rods at all core positions. The hydrogen loss from each element was then estimated by employing an extrapolation of 1200°F isothermal permeation data down to SNAP 10A operating conditions. The reactivity effect due to hydrogen loss was calculated to be -3 cents/year. Error analysis indicated an uncertainty in the calculated hydrogen leak rate of ±50%.

c. Fission Product Accumulation and Burnup

Fission product accumulation and U^{235} burnup were calculated with the SIZZLE computer code[5]. SIZZLE consists of a few-energy group (≤ 6) AIM-6 (one-dimensional diffusion theory) calculation of fission density and calculation of fission product accumulation by iteration for any number of time steps of specified length. The cross-sections used in the SIZZLE calculation were the "standard" library of 16-group material cross sections weighted over an ambient temperature zirconium hydride spectrum. The 16-group fission product cross sections were calculated from data reported in References 6 and 7. They were also weighted over a zirconium hydride spectrum. SIZZLE performs its own group reduction from 16 to ≤ 6 energy groups before beginning the iteration. The U^{235} burnup calculation was performed by simply reading in zero cross sections for all fission products. The effects of axial power distribution were accounted for in both fission product and burnup calculations. An estimate of the uncertainty in the calculation of fission products was made by hand calculating the reactivity effect using various sets of currently available fission product cross sections. The range of values indicated that the value calculated with SIZZLE (-9 cents/year) should be accurate within ±20%. A similar analysis indicated an uncertainty of ±20% in U^{235} burnup.

d. Prepoison Burnout

The Sm^{149} prepoison burnout was determined by calculating the worth of equilibrium fission product Sm^{149} and the worth of the prepoison loading. The calculations were performed with both the AIM-6[8] and DTK computer codes. The percent of equilibrium Sm^{149} concentration was calculated as a function of

time to determine the net change in total Sm^{149} worth with time. The Sm^{149} cross sections used were obtained from Reference 9. Effects of spectral shift with temperature, loading errors, self-shielding, and flux depression were evaluated and found to introduce an uncertainty of ±10% in Sm_2O_3 loading worth. It should be pointed out that an error of this magnitude, ±16 cents in SNAP 10A prepoison loading, is ±30% of the 53 cents calculated excess samarium in the core. Only about 31% of the excess Sm^{149} is burned out in 1 year of operation, so the burnout was expected to be 16.5 cents ± 5 cents.

e. Summary of Original Predictions

Table 6 (presented in Section V. A. 2. e) shows the calculated reactivity effects which were expected to occur during the 1-year static control period. Other reactivity effects were examined, but were found to be negligibly small. Radiation damage to the reactor structure, beryllium, fuel, and radiation shield was examined as were coolant flow distribution changes, grid plate deflection, and effects due to manufacturing and assembling tolerances. These effects were calculated, using the best analytical techniques and experimental data available, and were found to have a maximum total effect of less than 4 cents. Since the primary reactivity losses were -26 cents ±9.5 cents, it was concluded that the secondary effects were well within the uncertainty band of the primary effects and could be neglected until improved data were available.

The temperature drift during 1-year of operation was calculated using the LOAFER code. The primary reactivity loss mechanisms and Sm^{149} prepoison burnout were calculated as functions of temperature and time. The LOAFER model accounts for the reduction in reactivity loss rate resulting from a drop in temperature. The model assumed that xenon accumulation was completed in 72 hr, that the selected fraction of hydrogen redistribution was completed in 72 hr, and that the remainder of hydrogen redistribution was completed 15 days after the start of static control. This latter assumption was consistent with the HYTRAN calculation, since HYTRAN showed less than 1/2 cents of redistribution effect remaining at this time.

Figure 15 shows the predicted SNAP 10A temperature drift and the effect of accumulated uncertainties on the prediction. The predicted year-end temperature was $944\ ^{+42}_{-39}$ °F, when adjusted to the actual FS-3 average temperature at

the end of the 72 hr active control period. The less than ±5% uncertainty band was considered acceptably small for a preoperational prediction.

2. Performance Uncertainty Reevaluation

The reevaluation of S10FS-3 performance was begun after about 3 weeks of operation when it was observed that the reactor coolant temperature was decreasing more rapidly than had been predicted. All reactivity loss mechanisms were reexamined to determine whether or not the deviation from prediction could be accounted for. A description of the reexamination follows.

a. Hydrogen Loss

The reactivity loss due to hydrogen leakage was calculated, employing HYLO, to be -3 cents ± 1.5 cents/year. This calculation is based on 1200°F isothermal permeation test data which was extrapolated to SNAP 10A temperatures.

Experimental hydrogen loss data are available from SER, S2DR, and S8ER operation and from in-pile membrane tests, in addition to the isothermal element permeation tests.

Hydrogen loss rates from the operating SER[10] and S2DR,[11] as measured by reactivity losses, have been estimated variously at two to three times the rate predicted from the out-of-pile, as assembled, isothermal leak rates of the individual elements. The S8ER[12] on the other hand, showed an initial reactivity loss attributed to hydrogen loss that matched the predicted rate rather closely. Four irradiation capsules, the NAA 77 series,[13] were built and tested in the MTR in an attempt to measure the effect of reactor operation on the permeability characteristics of the coated cladding. If higher leak rates were caused by neutron and fission product bombardment of the coating, or by the presence of monatomic hydrogen produced by the reactor environment, it was hoped that the increase could be observed and measured. Results of long-time operation of three of these capsules again show leak rates two to three times above the last out-of-pile, as assembled, isothermal leak rates, but it has not been possible to separate the possible causes of these higher in-pile leak rates. Thermal aging causing coating crystallization, thermal shock after repeated thermal cycling, change of standardization in the measuring instrument, fuel-ceramic interaction, and mechanical damage have all been suggested as reasons for the higher leak rates.

It is concluded that the hydrogen loss rate in an operating system may be as much as three times greater than predictions based on isothermal permeation test data. Although hydrogen loss is a relatively minor effect in SNAP 10A, uncertainty in magnitude of the effect is relatively large.

Hydrogen loss becomes a larger reactivity loss effect at higher temperature and power conditions, however, the associated uncertainty in end-of-life temperature is not proportionally increased due to the strong temperature dependency of hydrogen leakage. Any drop in temperature slows the leakage, thereby limiting the effect. This effect is discussed in Appendix B.

b. Hydrogen Redistribution

Analysis of S10FS-3 reactivity losses during the active control period indicated that only about 3 cents of the losses were accountable to hydrogen redistribution. The analysis was based on the assumption that reflector movement effects occurred only during the first 17 hr at power (the time period when reflector heating occurred). The total calculated reactivity loss due to hydrogen redistribution was 22 cents ± ~ 6 cents. Therefore, 13 cents to 25 cents of the static control period reactivity losses could be attributed to hydrogen redistribution rather than the predicted 11 ± 6 cents. The preflight analysis indicated that hydrogen redistribution should be essentially completed within 21 days after reaching full power. The analysis of the time to completion of the effect was, however, considered to be the most uncertain part of the reactor performance.

Experimental data from S2DR, at fuel temperatures near S10FS-3 conditions, indicated that hydrogen redistribution was not completed more than 1200 hr after the start of the experiment. The indicated time constant (τ) was about 600 hr. At about 150°F above S10FS-3 conditions, hydrogen redistribution was observed to be essentially completed within 500 hr[8]. The indicated time constant for the high temperature case was 145 hr. S8ER experiments have indicated hydrogen redistribution time constants of about 28 hr at 1100°F T (inlet), 200°ΔT conditions.

Due to uncertainty in the analysis of S2DR data (resulting from separating hydrogen redistribution from other reactivity loss effects such as hydrogen loss, etc.) and the additional uncertainty resulting from the change in fuel element design (resulting in more severe axial temperature gradients in SNAP 10A),

the applicability of the S2DR hydrogen redistribution results to SNAP 10A was questioned. Consequently, the HYTRAN calculation of hydrogen redistribution reactivity effect and time constant were employed for predictions.

The HYTRAN calculation of hydrogen redistribution is based on the following equation:

$$J = -D\left(\frac{\partial N}{\partial r}\right) - D\left(\frac{NQ^*}{RT^2}\right)\left(\frac{\partial T}{\partial r}\right)$$

where

J = hydrogen current (moles H_2 /cm^2-sec)

D = diffusion coefficient for H_2 through the fuel alloy (cm^2/sec)

N = hydrogen concentration (H_{atoms} x 10^{22}/cm^3)

r = fuel rod radius (cm)

Q^* = heat of transport (cal. /mole)

T = absolute temperature (°K)

R = gas constant = 1.987 cal/mole-°K .

This model neglects axial diffusion within the fuel rod. This is a reasonable assumption since it takes about 20 times longer for a hydrogen atom to traverse the axial length of the rod than to migrate radially. Following radial migration, it is assumed that the hydrogen diffuses to a colder portion of the rod in the fuel rod-cladding gas gap. The hydrogen atoms then diffuse back into the fuel rod in the lower temperature regions of the rod. The HYTRAN code also assumes that there is no leakage of hydrogen through the barrier and cladding for the duration of the process. The HYTRAN calculation was repeated for each element in the core and summed to determine the total reactivity loss. The average hydrogen redistribution time constant calculated by HYTRAN was 91 hr.

The HYTRAN code was recently revised to permit more input/output flexibility. During the course of the revision process a logic error was discovered in the code. The diffusion coefficient calculated at the hot end of the fuel rod was the only one which was saved after the first itteration. As a result, the time constant calculated by HYTRAN was that associated with the hottest fuel. The cold end of the fuel element actually appears to determine

the hydrogen redistribution time constant because hydrogen must ultimately diffuse into that portion of the fuel material. The correction was made to calculate and save diffusion coefficients at each axial node. HYTRAN now calculates time constants of more than 3000 hr for equilibrium S10FS-3 hydrogen redistribution.

The correction of the hydrogen redistribution model is probably the most significant result of the FS-3 performance reevaluation. Hydrogen redistribution is not, however, important in high temperature (>1100°F inlet coolant temperature) reactors because the effect is essentially completed during the 3-day active control period.

c. Prepoison Uncertainties - Loading and Spectrum Effects

The Sm^{149} prepoison loading and worth is one of the larger uncertainties associated with SNAP 10A performance. An uncertainty in Sm^{149} loading of ±10% was estimated in predicting static control temperature drift.

A thorough analysis of the quality control and techniques employed in applying the prepoison showed that the uncertainty in total mg of Sm_2O_3 applied to the cladding tubes was about ±3% of the "quoted" value for any tube and within ±9% of the specified value. An additional uncertainty was introduced by the nonuniform distribution of the prepoison along the tube wall. Although the distribution seemed to be randomly high or low at the center of the tubes which were sampled, it is possible that a cluster of low-at-center or high-at-center tubes may be loaded into the central core positions of a SNAP 10A reactor. Nuclear self-shielding effects have been calculated to be about 3%, and flux level differences between the fuel and cladding are also about 3%. The combination of these effects was the basis for the assumed ±10% uncertainty in prepoison loading. Summing all uncertainties into a loading uncertainty was more conservative than calculating loading and worth errors separately.

A number of samarium worth experiments have been conducted with the SCA-4A critical assembly. A set of cladding tubes coated with various amounts of Sm_2O_3 (in the hydrogen barrier material) were placed in several core positions and the Sm^{149} worth was measured as a function of concentration and

position. The tubes were subsequently destructively analyzed to accurately determine the Sm_2O_3 loadings. Measured Sm_2O_3 worth was 0.83 cents/mg/in. in the core center position. An integration of the measured values over the core volume indicated an average worth of 17.7 cents/mg/in./core. This was in good agreement with the worth calculated with the DTK code (18.75 cents/mg Sm_2O_3/in./core). Other prepoison worth experiments were conducted in SNAP critical assemblies which resulted in measured worths of 15.6, 16.6, and 20 cents/mg Sm_2O_3/in./core.[14]

In summary, the experimental average Sm_2O_3 worth is 17.75 cents/mg/in./core with values ranging ±2.25 cents/mg/in./core from the average. An 8.0 mg Sm_2O_3/in. (average) loading would therefore be worth \$1.42 ± 18 cents. This may be taken as an indication that the total uncertainty in prepoison loading, distribution in the cladding tube, etc., is about ±13%. This is, therefore, assumed as the prepoison loading uncertainty rather than the ±10% used in the original predictions. In the following discussion, the original DTK calculations with ±10% uncertainty are compared to prepoison worth based on the experimental data and its ±13% uncertainty.

The average Sm_2O_3 loading of S10FS-3 was 8.75 mg/in., or \$1.64 using the DTK code. When corrected for self-shielding in the three high Sm elements (nominal 16 mg/in.), flux depression in the barrier material relative to the fuel, and the centralized location of the high Sm elements, the adjusted worth is \$1.62 ± \$0.16. Using the experimental worths, discussed in preceeding paragraphs, an estimate of the S10FS-3 loading worth would be \$1.55 ± \$0.20.

Using known values for the yield of promethium^{149}, the worth of equilibrium Sm^{149} in the SNAP 10A reactor can be shown to be \$1.09. Subtracting this value from the initial loading worth gives the initial excess samarium worth. The initial excess is, therefore, \$0.53 ± .16 using DTK results and \$0.46 ± .20 using the experimental results.

The fraction of the excess Sm^{149} which is burned out in a year at 40 kwt is simply:

$$F = 1 - e^{-\lambda t} = 0.312,$$

where λ^{-1} = Sm^{149} time constant = 936,000 kwh, and t = operating time in kwh = 350,000 kwh.

The expected reactivity gain in 1 year due to prepoison burnout is 16.5 cents ± 5.0 cents using DTK worths. The experimental data result in a calculated reactivity gain of 14.4 cents ± 6.2 cents. The latter values, since they were obtained from critical experiment data, represent the total effect of Sm^{149} prepoison loading and ambient spectrum worth uncertainty on the expected reactivity gain.

An additional uncertainty is introduced into the values for reactivity gain by changes in the neutron spectrum between ambient and operating temperatures. Two theoretical models which describe neutron thermalization in zirconium hydride are available.[15, 16] Recent experimental data[17] show that neither of the models correctly account for changes in neutron energy spectrum due to changes from ambient temperature. The QUICKIE[18] code has been used to weight material cross sections over the zirconium hydride spectrum. The spectral effect on Sm^{149} worth, due to a temperature change from ambient to 1200°F, was calculated to be only about -3% using QUICKIE. This was included as part of the total uncertainty in the original predictions.

The experimental neutron energy spectrum data of Young, et al,[17] for boron poisoned zirconium hydride indicated a significant spectral shift from ambient conditions to 876°F. This spectral shift results in an effective reduction in samarium prepoison worth with increasing temperature. The experimental data were for boron absorber contents equivalent to 3.4 and 8.0 barns per hydrogen atom. The U^{235} content of SNAP 10A may be considered an absorber equivalent to 15.8 barns per hydrogen atom. The experimental data show an increasingly larger spectral effect on prepoison worth for higher absorber content; however, the 8.0 barns per hydrogen atom spectral values were employed in the current performance evaluation because they were the best approximations to the SNAP 10A spectrum currently available.

Changes in the average one-energy group cross sections were calculated assuming that the spectrum was unaffected by temperature changes for energies above 0.6 ev. The experimental data[17] show no change in spectrum with temperature for energies between 0.6 ev and 1 ev and does not extend above 1 ev. The results were a 16% change in the samarium cross section and 9% change in the U^{235} fission cross section in the energy region 0.01 ev to 0.6 ev. Approximately 65% of thermal fissions are caused by neutrons in this energy range so

the effective change in the one-energy-group uranium-235 fission cross section was only 5%. Since the reactivity worth of samarium is proportional to the ratio of samarium cross section to fission corss section, the effective worth of samarium is reduced by 10%. This number could vary between 5% and 15%, however, due to the uncertainty in the application of the experimental data to the SNAP 10A spectrum. The change in spectrum also causes the calculated fraction of the excess Sm^{149} burned out in a year to decrease from 0.312 to 0.286 ± .013.

Table 4 shows the effect of spectral shift, with temperature, on both calculated and experimental prepoison worths. The uncertainty in spectral effect was assumed independent of the uncertainty in ambient spectrum loading worth and the two were combined statistically to obtain the uncertainties in the table.

It appears that the rate of prepoison burnout could be significantly in error due to failure of the QUICKIE model to correctly account for the spectral shift with temperature. Since the H/Zr ratio and boron content used in the spectal shift experiment[17] were significantly different from SNAP 10A conditions, and since the temperature range studied was below SNAP 10A operating conditions, it is evident that more experimental data or an improved thermalization model are required before the effect of spectral shift on SNAP 10A prepoison burnout can be accurately determined.

TABLE 4

REEVALUATION OF Sm^{149} PREPOISON BURNUP IN S10FS-3

	Ambient Spectrum	876°F Spectrum
Initial Loading		
Worth, ¢ (DTK, 40 kwt)	162 ± 16	147 ± 17
(Experiments)	155 ± 20	139 ± 20
Loading in Excess of Equilibrium		
Worth, ¢ (DTK, 40 kwt)	53 ± 16	38 ± 17
(Experiments)	46 ± 20	30 ± 20
Reactivity Gain/Year		
Worth, ¢ (DTK, 40 kwt)	16.5 ± 5.0	10.9 ± 5.0
(Experiments)	14.4 ± 6.2	8.6 ± 5.9

The observed temperature drift behavior of S10FS-4 was very nearly the same as that of S10FS-3.[2] This indicates that even though a detailed explanation of this drift is not available at this time, it is possible with come degree of confidence to predict the end-of-life temperature of future reactors of the SNAP type operating under similar conditions.

d. Other Contributing Effects

(1) S10FS-3 Reflector Motion

As discussed in Appendix A, the reflector mounting on FS-3 was modified to allow remote removal of the reflector. These modifications allowed the reflector to move abnormally during periods of differential expansion between the vessel and reflector. It was estimated (Section III-C) that 16 ± 4 cents of reactivity was added during the startup period due to this abnormal reflector motion. It is estimated (Section IV-B) that 11 cents ± 2 cents of reactivity was removed by reflector movement during the active control period. The limit switch indications showed that one reflector half returned to its normal position 17 hr after startup, while the other returned after 100 days of power operation. Apparently, abnormal movement of only one reflector half affected the reactor operation during the endurance period. If it were assumed that this reflector half and the vessel reached thermal equilibrium with no relative movement at the upper support points, the reflector half would be displaced an amount equivalent to 4 cents or 13°F. This amount is estimated to be approximately that removed by gradual motion during the 100-day period.

This reactivity loss apparently occurred almost completely during the first 10 days of static control operation, as indicated by the temperature derivative data (Figure 16). Because of the uncertainty in this evaluation, however, the possibility that no reactivity was associated with the uplifted reflector must also be recognized. Therefore, an uncertainty of ± 4 cents was assigned to this effect in the reevaluation.

(2) Fuel Burnup and Fission Product Accumulation

(a) U^{235} Burnup

Burnup of fissionable material depends on the power level, energy release per fission and spatial worth of the material. The new value for reactivity loss due to burnup of 3.6 cents/year was calculated using an average power

level of 39.5 kwt, slightly higher than that used in the original predictions. An uncertainty of ± 0.7 cents/year was assigned to this value after calculations showed a maximum fuel burnup of 4.3 cents/year was possible at the S10FS-3 conditions by using pessimistically high absorption cross sections.

(b) Fission Product Accumulation

The reactivity effect due to fission product poisoning was originally calculated using fission product cross sections obtained from the GAM-I tape (energies > 0.4 ev),[6] and from the Garrison and Roos report (energies > 0.4 ev).[7] The reactivity effect, as previously noted, was 9 cents/year.

A more recent set of cross sections has recently been compiled from the GAM-II tape and Nephew's data.[19] Calculations have been completed, using the new cross sections, which indicate about -10.5 cents/year reactivity loss. These results indicate that the assumption of an uncertainty in fission product poisoning of 20% was probably adequate. The best current estimate for this effect is 11 ± 2 cents/year.

(3) Radiation Damage to Components

Radiation damage to all reactor components was examined and no significant effect was found in any area during the original analysis. All components have been re-evaluated and the effects determined.

Recent experimental data on the radiation damage effect of fast neutrons on cold pressed LiH indicates that a significant amount of radiation shield swelling may occur at SNAP 10A flux and temperature levels.[20] Shield swelling results in reduced density of the LiH nearest the core and, hence, a reduction in the number of neutrons reflected back to the reactor. The calculated maximum reactivity effects due to shield swelling are included in Table 5, following. It was concluded that the maximum contribution to reactivity losses during the static control period due to radiation shield swelling might be 1.2 cents, while only about 0.4 cents of this total might occur during the last 9 months of operation.

The effect of beryllium metal swelling is very similar to the radiation shield swelling phenomenon. The maximum reactivity loss calculated for Be swelling was << 0.5 cents/year.

TABLE 5

REACTIVITY LOSS DUE TO SHIELD SWELLING

Time From Full Power (days)	Maximum Reactivity Loss (¢)
3	0.6
5	0.8
10	0.9
20	1.0
40	1.2
90	1.4
365	1.8

Fuel element swelling due to radiation damage, another relatively minor reactivity loss mechanism, is calculated to be $<< 0.75$ cents/year.

The sum of all radiation damage effects is only about 2 cents/year, with nearly one-third of the effect occurring in the 3-day active control period.

(4) Thermal Effects

(a) Change in Thermal Conductance

An increase in thermal resistance between the fuel and the coolant would result in a decrease in reactivity. Therefore, the possibility of a change in the overall thermal conductivity, UA, has been evaluated.

The nominal value of UA in SNAP 10A is 1.29 kw/°F. The overall resistance (1/UA) consists of the following individual resistances:

Coolant film	24%
Clad	3%
Hydrogen barrier	9%
Gas gap	30%
Fuel	34%

The resistance of the coolant film could increase significantly only by a change in the wetting characteristics of the surface or by the deposition of a fouling film on the elements. Neither of these mechanisms is likely to have occurred.

The clad and hydrogen barrier contribute relatively little to the overall thermal resistance. There is no reason to believe that their conductance has changed appreciably. The resistance of the gas gap could change by two mechanisms: a change in the thermal conductivity of the gas, or a change in the gap width. The gas in the gap is predominantly hydrogen. The addition of other gases in appreciable concentrations would reduce the conductivity. The concentration of fission product gases, such as xenon, krypton, or iodine; however, is expected to be minute so that the gas conductivity should not have changed materially. The local width of the gap, on the other hand, is likely to have changed as a result of hydrogen redistribution. The density of the fuel increases as hydrogen concentration decreases, leading to a local reduction in fuel diameter and an increase in gap width. As a result of hydrogen redistribution, the average gap width increased 1.6×10^{-4} in. at the axial midplane of the core, 4.3×10^{-4} in. at the downstream end and approximately 0.3×10^{-4} in. for the core average. The corresponding increases in the local thermal resistance between fuel and coolant are 3% at midplane, 6% at the exit end and negligible on the average.

On the basis of past experience in the testing of SNAP fuel elements, it is assumed that the FS-3 elements are retaining their integrity without serious cracking. Any change in the fuel resistance, therefore, would have to be due to a change in thermal conductivity. There is evidence that the conductivity of the fuel is dependent on hydrogen concentration with a reduction of about 3% in thermal conductivity per 0.01 reduction in H/Zr ratio.[21] Hydrogen redistribution produced decreases of 0.01 and 0.03 in the average H/Zr ratios at the reactor midplane and the downstream end leading to decreases in the fuel conductivity of 3% and 9% and decreases in the local overall thermal conductance between fuel and coolant of 1% and 3%, respectively. (Hydrogen loss was assumed negligible so that the core average H/Zr ratio remained unchanged at 1.82.)

The maximum credible reduction in the overall thermal conductance between fuel and coolant, UA, due to the combined effects of hydrogen redistribution on fuel conductivity and gap width is seen to be less than 5%. A 5% reduction in UA would result in an increase of 1.6°F in the difference between average coolant and average fuel temperatures. The maximum combined reactivity effect would be less than 0.2 cents or about 0.6°F.

(b) Coolant Flow Distribution Effects

The bottom plate of the SNAP 10A low grid plate was orificed in an attempt to obtain a flow distribution matching the core radial power distribution, which would result in equal coolant temperature rise in all channels. Flow distribution tests indicated that the orifice plate was relatively ineffective because of flow mixing between the lower orifice plate and the support plate, cross-flow within the core, and nonuniform velocity distributions in the core plenums. In order to be conservative, all SNAP 10A thermal calculations have assumed a uniform flow distribution in the core and no mixing or cross-flow between channels. The corresponding maximum hot-element fuel temperature exceeds the core average coolant temperature by 135°F for a core coolant temperature rise of 128°F. In a core with a uniform outlet temperature, the maximum fuel temperature would be 29°F less, resulting in a small positive reactivity insertion of the order of 1.0 cents.

The assumption of uniform flow distribution with no mixing is considered conservative. If a more pessimistic situation is postulated, namely, a condition in which the coolant velocity in the central channels is 10% below the core average, the maximum fuel temperature could exceed the predicted temperature by 13°F, resulting in a reactivity reduction of about 0.5 cents.

The possibility of a major flow blockage in a coolant channel, causing a local fuel hot spot, is exceedingly remote. In the first place, the source of the blocking solid is difficult to visualize. Secondly, since all coolant channels are connected, the sealing of an orifice hole or the lodging of a plug in a channel would not lead to flow stagnation in the channel. Thirdly, the NaK is a sufficiently good thermal conductor that stagnation in one of the blind channels adjacent to the internal reflector, for example, would not produce a significant fuel temperature increase.

What is of primary concern is not the uncertainty of flow distribution or orificing effectiveness, but the possibility of a gradual and continuous change in the flow pattern. None of the effects discussed above would appear to lend themselves to producing this type of change. Whatever the effectiveness of the orificing arrangement, it is not likely to change during reactor operation. A solid plug lodging in a channel would produce its effect, if any, virtually instantaneously, and not gradually over a period of time. There is no evidence to indicate

TABLE 6

COMPARISON OF PREFLIGHT, REEVALUATED, AND "BEST-FIT" STATIC CONTROL PERIOD REACTIVITY LOSSES FOR CONSTANT POWER CONDITION

Reactivity Loss Mechanisms	Reactivity Effect and Uncertainty (¢/yr at 40 kw)		
	Preflight Prediction	Reevaluated	"Best-fit" Values
Primary Effects			
Hydrogen Loss	-3 ± 1.5	$-3 \pm {}^{0}_{6}$	-2.5
Hydrogen Redistribution	-11 ± 6	-19 ± 6	-18.
Prepoison Burnout	$+16.5 \pm 5$	$+8.6 \pm 5.9$	+15.3†
Other Effects			
Reflector Motion	Not considered	-4 ± 4	-5
U^{235} Burnup and Fission Product Accumulation	-12 ± 2	-14.6 ± 2.7	-11.9
Component Radiation Damage	0	-1 ± 1	0
Thermal Effects	0	$0 \pm {}^{0}_{0.2}$	0
Total	-9.5 ± 8.2	$-33 \pm {}^{9.8}_{11.5}$	-22.1

†Loading worth of $1.50 (hot) was assumed

that there could be a gradual selective buildup of a plug or a fouling film or a continuous gross distortion of the fuel elements, the internal reflector or the core vessel; these are the only mechanisms that come to mind in postulating a continuous change in flow distribution.

e. Summary of Current Performance Evaluation

A summary of the reevaluated SNAP 10A static control period reactivity losses is shown in Table 6. The values are normalized to 40-kw operation for 1 year for comparison to the pretest predictions. The most significant changes are evident in the prepoison burnout (reduced) and hydrogen redistribution (increased) effects. The uncertainty in the total of the calculated reactivity losses was determined by the "square root of the sum of the squares" method, which

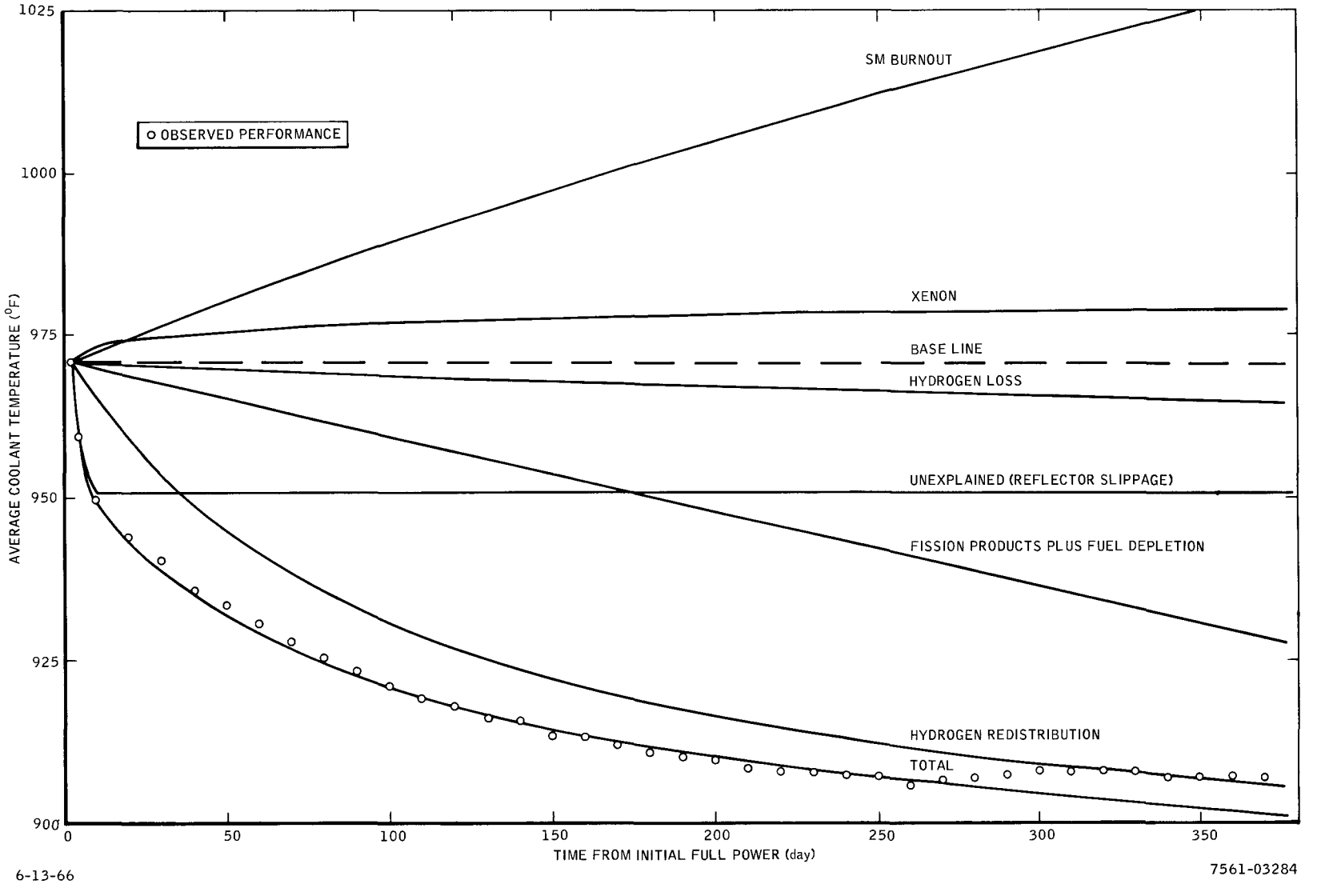

Figure 18. "Best Fit" Model for Static Control Period Reactivity Losses

implies that all effects are independent. In fact, this assumption is not correct and the analytical uncertainty should be larger than the indicated values.

A computer code (DUMOR) was written to include calculation of each of the major reactivity effects as affected by reactor performance. The code calculates the sum of all reactivity effects over a short-time interval ($\leq$ 24 hr) and determines the resulting temperature and power level for use in the subsequent time step through temperature and power reactivity coefficients. The hydrogen redistribution time constant and magnitude of effect, and the magnitude of prepoison burnout, were varied to obtain a fit to observed reactor performance. The best fit is compared to FS-3 performance data in Figure 18. This fit matches the observed performance closely except for the "unexplained" positive drift between 250 and 300 days. Also shown in the figure is the reactivity gain or loss (in °F) attributed to each reactivity effect. The reactivity effects employed to obtain the fit are shown in Table 6. The values tabulated are for 40-kw, 1-yr operation, for comparison with the reevaluated values. Because of the downward drift in reactor power, the xenon concentration decreased during the operation, adding reactivity, as shown in the figure. Table 6 does not show this effect as it is normalized to constant power. Agreement between "best-fit" values and the analytical values shown in Table 6 is seen to be quite good. This is taken as an indication that the analytical model employed in DUMOR is useful in predicting SNAP 10A reactor performance.

The same DUMOR model shown in Table 6 (but without reflector movement) was used to calculate the S10FS-4 reactor performance. The agreement between calculated and observed performance was excellent, and tends to justify the assumptions of reflector slippage early in FS-3 operation.

In summary, the observed performance of FS-3 has been analyzed in detail to determine the cause for deviation from the preflight predictions. It has been concluded that a long hydrogen redistribution time constant at 900°F inlet temperature and spectral shift and prepoison loading uncertainties were the principal contributors to the performance deviations. Neither of these effects is as important for high temperature static controlled reactors for reasons described in Appendix B.

An analytical model has been programmed for digital computer solution of the performance of S10FS-3 and similar statically controlled reactors.

B. DIAGNOSTIC SYSTEM PERFORMANCE

1. Limit Switches

On May 2, after 100 days at full power PnS-16, the -Z reflector ON-OFF switch, switched open giving a "reflector on" indication. All other switches continued to read normally.

2. Control Drum Position Indicating System

Table 7 tabulates indicated positions of all four drums at approximately 1 month intervals since the end of the active control period on January 25, 1965. All data points are in volts, and represent the output of the demodulators, each point being the average of 20 readings covering a time period from 6 to midnight

TABLE 7

FS-3 DRUM POSITION SENSOR CHANNEL OUTPUT SIGNALS (volts)

Date	Fine Drum No. 3		Fine Drum No. 4		Coarse Drum No. 1		Coarse Drum No. 2	
	PnI-1 (0-135° Range)	PnI-6 (0-30° Range)	PnI-2	PnI-3	PnI-105	PnI-108	PnI-106	PnI-107
1/25/65	4.0397	0.4615	4.0906	0.7785	5.1013	5.8928	4.9293	5.0252
2/1	4.0404	0.4645	4.0905	0.7726	5.1042	5.9109	4.8947	4.8589
3/1	4.0499	0.5197	4.0936	0.7838	5.0920	5.8579	4.8793	4.8057
4/1	4.0571	0.5481	4.0979	0.7986	5.1122	5.9410	4.8776	4.7923
5/1	4.0613	0.5756	4.1000	0.8119	5.1131	5.9474	4.8726	4.7706
6/1	4.0632	0.5976	4.1078	0.8277	5.1049	5.9316	4.8836	4.8232
7/1	4.0615	0.5974	4.1059	0.8414	5.1079	5.9500	4.8715	4.7614
8/1	4.0625	0.6104	4.1088	0.8483	5.1029	5.9320	4.8708	4.7735
9/1	4.0629	0.6125	4.1110	0.8604	5.1091	5.9452	4.8701	4.7717
10/1	4.0640	0.6035	4.1173	0.8873	5.108	5.9345	4.8726	4.7573
11/1	4.0646	0.5920	4.1165	0.8933	5.111	5.9420	4.8795	4.8087
12/1	4.0650	0.6158	4.1223	0.9025	5.117	5.9765	4.8680	4.7473
1/1/66	4.0660	0.6150	4.1235	0.9059	5.113	5.9570	4.8940	4.8708
2/1	4.0656	0.6155	4.1270	0.9300	5.1105	*	4.8612	4.7275
2/15	4.0668	0.6197	4.1292	0.9376	5.112	*	4.8720	4.7570
Total shift (volts) and direction	0.027(+)	0.158(+)	0.039(+)	0.159(+)	0.0107(+)	0.0642(+)	0.0573(-)	0.2682(-)
Total shift (equivalent degrees arc)	0.811(in)	0.948(in)	1.17(in)	0.955(in)	0.321(in)	0.385(in)	1.72(out)	1.61(out)

*Data logger temporarily out of calibration on this channel.

of the day indicated. Table 7 shows that all channels showed continuous change, or drift, with time. In most cases the change was positive, with the exception of PnI-106 and -107, (coarse drum No. 2) for which the change was negative, and also the largest in magnitude. There are a number of possible causes for the output changes observed, including the following:

1) Changes in the resistance of the sensor primary circuit, in the sensor primary winding itself or in the cabling. Winding changes could be due to radiation effects on the copper wire or its nickel cladding, or from diffusion of the nickel into the copper. In the cable, changes could be due to variation of the contact resistance of the connectors, and less likely, from changes in resistance of the wire itself.

2) Changes in the resistive or reactive components of the sensor input impedance, caused by variations in the resistivity or magnetic properties of the sensor structure.

3) Mechanical shift of the sensor rotor with respect to the stator, could result from: (a) changes in the configuration or force generated by either the sensor shaft-loading Belleville spring or the spring in the flexible coupling between the sensor shaft and the drum bearing shaft, or (b) radiation-induced growth of metal parts in the sensor or its mounting assembly. In this regard it should be noted that on the S10-FS-3 reactor the sensor shafts on the coarse drums were subjected to the proper tension loading, but the fine drum sensor shafts were not.

These various possibilities were investigated, and the following information obtained and conclusions reached.

1) Significant changes in sensor primary winding resistance, either from displacements or transmutations in the copper or nickel, are not likely. The operating temperature of the sensors (375 F) is high enough to anneal out all defects in copper and transmutation effects were ruled out. This is considerably less than the ~19% change which it is calculated would be required to produce the 1% change observed in the channel outputs. Also, data from the manufacturers of nickel-clad copper wire indicated that the diffusion of nickel into the copper is not a problem until the operating temperature is at least 500°F. Data from the HF-5 irradiation test in which sensors were irradiated

to $>10^{18}$ nvt and 10^{9} R gamma at 500°F corroborated this, showing a maximum increase in sensor primary resistance of only 5% (instrument accuracy, ±3%).

2) Discussions with D. I. Gordon of the Naval Ordnance Laboratory at Silver Spring, Maryland, verified the fact that neither resistive or reactive components of the sensor input impedance would be expected to change significantly due to the effects of either radiation or temperature on the magnetic material in the sensor.

3) The possibility of increases in the contact resistance of the pins in the cable connectors is considered a real one. This is based on the fact that similar effects were observed in the S10FSM-1 system test and in laboratory "poor vacuum" tests. The fact that air was deliberately bled into the S10FS-3 test vacuum chamber further increased the possibility of this occurring. However, in engineering tests where resistance was added in series with the sensor primary, the demodulator output decreased in all cases. Therefore this effect would explain the drift of coarse drum No. 2 sensor only.

4) Tests of the effect of shaft axial loading on sensor output showed that:

a) A compression load on the shaft causes the armature to move at the rate of, 0.000367 in./lb and results in a demodulator output decrease at the rate of 16 mv (0.43° arc) per mil.

b) A tension load on the shaft causes the armature to move at the rate of 0.0003 in./lb and results in a demodulator output increase at the same rate as in (a). However, from the no-load condition, only 0.0004 in. motion is possible with 3 lb of tension load.

The direction of change of demodulator output observed in the FS-3 test was positive for which the data in (b) applies. However, as stated previously, starting from the no-load condition it is not possible to cause the almost 1° shift observed by pulling on the shaft. A possible explanation would be that during installation of the sensors they were inadvertently subjected to a compressive load which was relieved during the test period by a decrease in the force exerted by the shaft coupling spring. Another would be that an equivalent relative motion between armature and stator occurred due to radiation-induced growth on the Type 416 SS sensor housing.

In summary, the gradual shift of sensor output signal shown in Table 7 is believed caused by either (1) mechanical shift of the sensor armature with respect to the stator, due to changes in configuration or force characteristics of the springs in the shaft drive train, or radiation-induced growth of the Type 416 SS sensor housing or titanium sensor mounting yoke, or (2) by increases in contact resistance of the cable connector pins, due to oxidation or contamination. (Applicable to Sensor No. 2 only.)

It should be noted that the performance of the sensor channels on S10FS-3 is not truly representative of what would occur on a flight system, for two reasons: (1) Since the demodulators are not in the instrument compartment and are therefore not exposed to the radiation environment, no shift has been caused by them; whereas with the present 10A demodulator design, drift would occur in a radiation environment beginning at about 10^{13} nvt fast neutrons. (2) On a flight system, presumably the sensor shafts would be subjected to tension loading and drift due to differential expansion or radiation effects on springs, etc., would be minimized.

C. CONTROL SYSTEM PERFORMANCE

During the endurance period, the control system is inactive unless reactivated for special test purposes.

The S10FS-3 temperature switches were observed after the active control period to determine the temperature at which they again opened as the temperature drifted downward. The switch with the higher set point opened at 1005°F. This set point is essentially the same as the 1007°F point indicated at the end of the active control period.

The timer was operated after 21 days and was within tolerance on both the 1-min and 1-hr time bases. Because of the high radiation in the vacuum chamber, due to scattering off the walls, the timer had received about the same dose as is expected in 1 yr of a flight test. The timer could not be reset externally, so no further testing was performed.

The temperature detectors used to control the reactor, TS-3T and TS-4T, were disconnected from their respective switches on February 19 and their resistances were subsequently taken daily. Figure 19 shows the initial and final detector resistance characteristics of TS-3T and TS-4T. Detector resistance is shown as a function of reactor outlet coolant temperature as indicated by

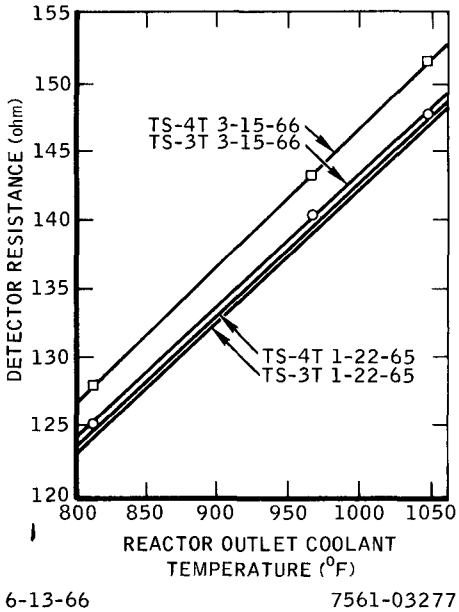

Figure 19. Temperature Detector Performance During Static Control Period

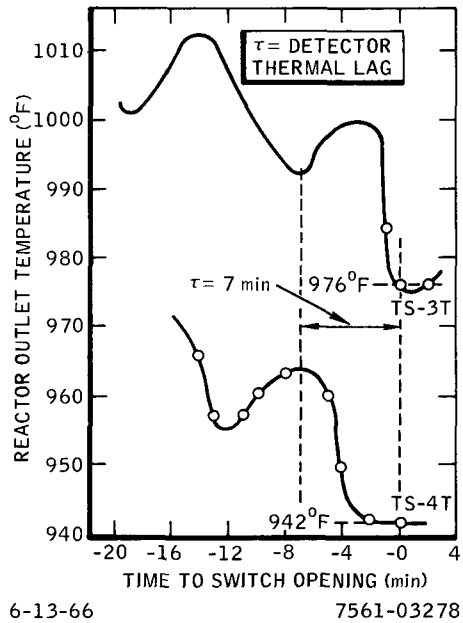

Figure 20. Reactor Outlet Temperature During Cool-Down Immediately Prior to Temperature Switch Actuation

thermocouples. Inspection of Figure 19 indicates that the resistance of detector TS-3T increased by about 0.8 ohm during the period between calibrations (over one year). The resistance of detector TS-4T increased by about 3.8 ohm during the same period. Determination of the absolute drift in detector resistance is, of course, dependent on the stability and accuracy of the thermocouple temperature measurements. The relative detector drift of 3.0 ohms, however, is independent of these errors and is clearly evident from Figure 19.

Because of the importance of the data taken during shutdown to the temperature detector analysis, the complete discussion of the detector performance will be presented here. This provides a more continuous and easier to read discussion.

Prior to system cool-down the temperature detectors were reconnected to the temperature switches to determine the final temperature seitchpoints. When the system was cooled down TS-3T and TS-4T switched at indicated reactor outlet coolant temperatures of 975°F and 942°F, respectively. The reactor coolant outlet temperature history immediately prior to each temperature switch actuation is shown in Figure 20 for TS-3T and TS-4T. If it is assumed that the detectors had a thermal lag during cool-down of approximately 7 min, then the corresponding detector temperatures at the switch set point may be approximated

as the coolant temperature about 7 min prior to switch opening. The corresponding detector temperatures at the switch point, as determined from Figure 20, are 992°F and 964°F for TS-3T and TS-4T, respectively. The detector resistances corresponding to these temperatures are 142.2 ohms and 142.6 ohms for TS-3T and TS-4T, respectively. These resistances agree closely with the temperature detector resistances of 142.54 ohms and 142.62 ohms required to drop out the TS-3 and TS-4 temperature switches, respectively, which were determined during the realignment of the switch set points on January 22, 1965.

Measurements of switch set points after system cool-down verified that the switch set points did not change. Therefore, when proper allowance for detector thermal lag and changes in detector characteristics are made, it is clear that performance of the temperature switches was completely acceptable.

It is not immediately apparent why the detector circuit resistance of TS-4T experienced a positive resistance increase approximately 3.0 ohms greater than that indicated for TS-3T. Resistance measurements were taken daily throughout the test on two additional temperature detectors which were installed in thermowells adjacent to the reactor control temperature detectors. These thermowells normally contain the high and low temperature switches used in the malfunction detection circuits of the flight system.

Figure 21 shows the resistance versus temperature and time history of all four of the detector circuits. The dashed lines indicate the initial detector resistances versus coolant temperature characteristics. It is interesting to note that the initial and final rate of change of resistance versus temperature are equal for each of the detector circuits. The slight differences in slope between TS-2T and the other detectors is probably the result of individual detector installation thermal characteristics. The fact that the slope for a given circuit did not change after more than a year of operation, indicates that the sensitive resistance element did not experience contamination or degradation that would produce a change in the temperature coefficient of resistance (α) of the element material. The resistance of detector circuits for TS-1T and TS-3T remained equal to each other at any given temperature within a fraction of an ohm (~0.4) for the entire test period.

The resistance of the detector circuit at a given coolant temperature can increase as the result of:

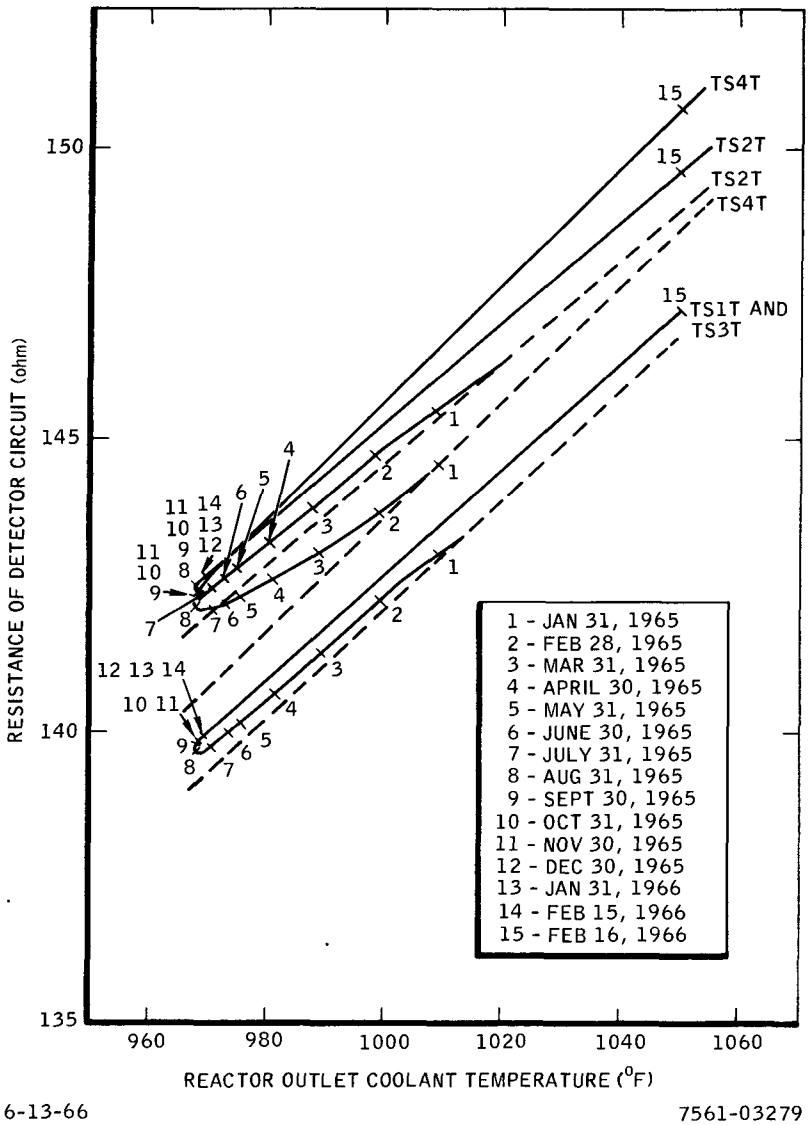

Figure 21. Resistance-Temperature-Time Performance of S10FS-3 Temperature Detector Circuits

1. increase in detector resistance
2. increase in connector contact resistance
3. increase in lead wire resistance
4. changes in detector installation errors.

Experience with other temperature detectors in developmental and qualification testing, indicates that expected changes in detector resistance as the result of temperature and radiation exposure would be on the order of about 0.15 ohms rather than the 3.8 ohms indicated for TS-4T. Increases in connector contact resistance as the result of temperature and time dependent oxidation of connector contract surfaces and changes in contact spring force resulting from realization of contact material could also result in increased detector circuit resistance. Uniform degradation of contract resistance will not influence the measured detector resistance or the performance of the temperature switch. Non-uniform degradation of all three high temperature contacts in a detector connector, however, can result in apparent increased detector resistance as measured and can also result in changes in temperature detector set point. Similar results can occur as the result of lead wire resistance changes. Measurements of detector circuit resistance during system cool-down indicated that the lead wire circuit resistance on detector TS-3T may have increased as much as 0.5 ohms from the initial lead wire circuit resistance measured at the same coolant temperature. Similar measurements on detector TS-4T indicate that lead wire circuit resistance increases at about 0.33 ohms may have occurred during the test. External measurements of detector circuit resistance cannot yield data to resolve detector drift, differential contact resistance changes, or differential lead wire resistance change effects. These measurements can only indicate total resistance changes.

Changes in detector installation errors can result in appreciable changes in detector resistance at a given coolant temperature. The detector installation design is such that the detector resistance can be from 5 to 10 ohms below that of an isothermal detector element at the coolant temperature. Variation in thermal radiation view temperatures, heat transfer coefficients from the detector head and thermal conductivities and emissivities between the heat source and the resistance element can result in changes in installation errors.

It is suspected that the detector circuit changes indicated for the detector are the results of combinations of the above causes. The greatest contributions to resistance change, however, are expected to be differential contact resistance changes and changes in installation errors resulting from changes in heat transfer conditions which determine the relationship between average detector temperature and coolant temperature.

Daily checks of the coarse control drum actuators for movement about their full-in position utilizing a manual controller indicated consistent satisfactory operation of the actuators and bearings. The coarse control drum actuators operated at a temperature of approximately 250°F throughout the test.

VI. EXTENDED OPERATION AND SHUTDOWN

On February 16, 1966, after 390 days of continuous operation, the FS-3 power and temperature were increased to approximately the startup conditions. The reactor was actively controlled for 72 hr and then statically controlled until March 15, 1966, when the system was shut down.

This perturbation of FS-3 normal operation was originally conceived as a year-long sequence of operations at various power levels and corresponding temperatures, which were designed to provide hydrogen loss rate and hydrogen redistribution information. Funding, however, limited operation to the 28-day test described in this section.

A considerable amount of useful information was obtained during the perturbation test: 1) the reliability of the reactor system after extended operation was demonstrated; 2) the reactivity lost during endurance period operation was measured; 3) control system operation after extended inactivity was demonstrated; and 4) diagnostic instrumentation performance was demonstrated.

The reactor shut-down, after more than 10,000 hr of continuous full-power operation, was uneventful.

A. REACTOR PERFORMANCE

1. Power Increase Phase

It was predicted that 20.3¢ of reactivity would have to be inserted to increase the average coolant temperature to 980°F, and the power to 44 kw. The observed reactivity insertions totalled 17.4¢. The reactor was not stabilized at the time of achieving the 44-kw level because xenon was not at equilibrium and the reflector temperature was increasing. When the calculated losses due to xenon and reflector effects are added to the reactivity insertions, an effective power coefficient of -0.29 (±0.02) ¢/°F is obtained. This is significantly lower than the -0.334¢/°F which had been used in previous analysis of endurance period reactivity losses. An isothermal temperature coefficient of -0.25 (±0.02) ¢/°F was also indicated by the data.

This power level change was somewhat more useful for the determination of temperature coefficients than the initial reactor startup because the uncertainty due to reflector motion was apparently not present, as indicated by no reflector ejection indications.

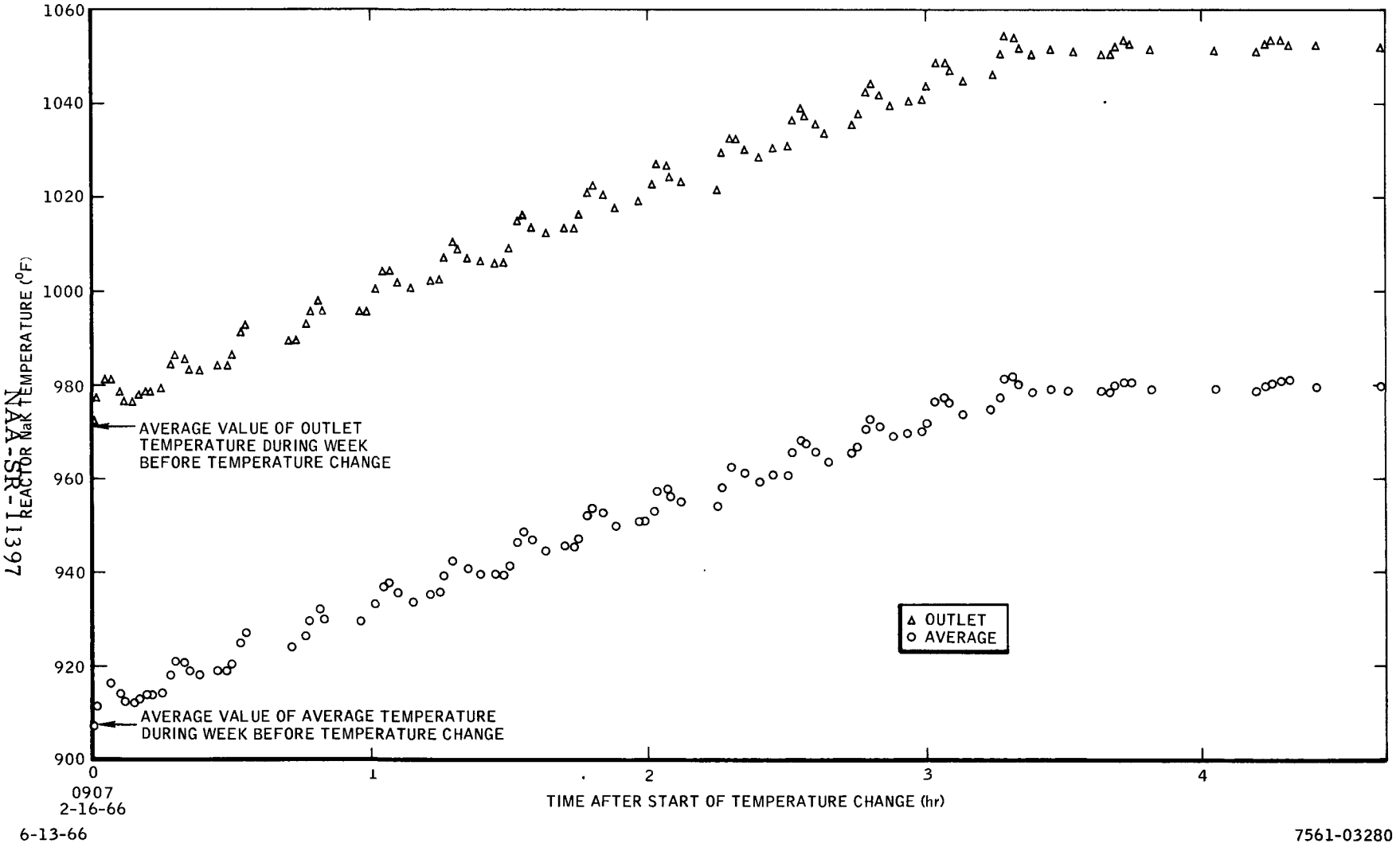

Figure 22. Reactor Performance During Extended Operation Test Power Level Change

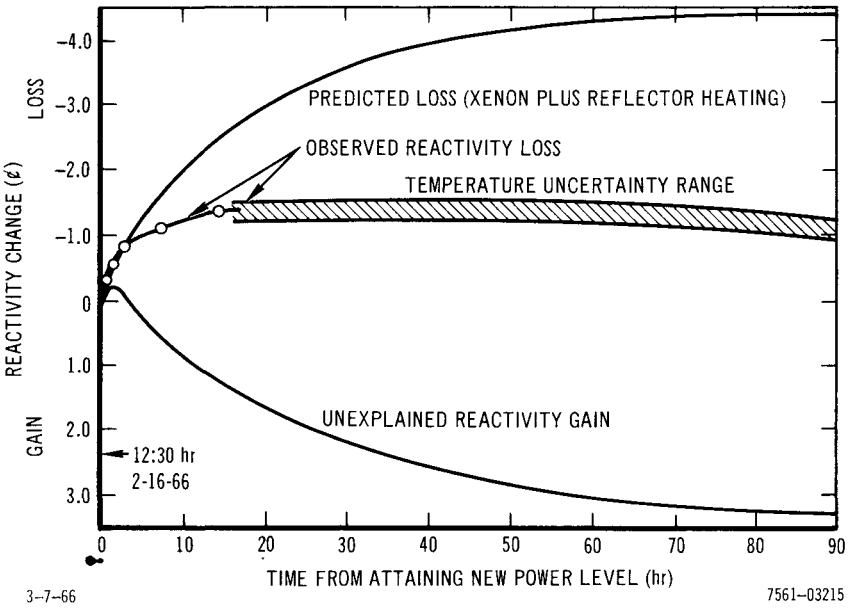

Figure 23. Reactivity Loss During Active Control After Power Level Change

Reactor temperature performance during the power increase is shown in Figure 22. The reactivity insertions are apparent as "bumps" in the temperature increase curve.

2. Active Control Phase

Three and one half hours after initiation of the perturbation test, active control was commenced. It was anticipated that 4.3¢ of reactivity would be required to maintain test temperature and power during the 72-hr period. The observed reactivity loss was only about -1.3¢ during the first 15 hr of the active control period, followed by a small ($\sim$ +0.1¢) reactivity gain during the remaining 57 hr. An unexplained 3.1¢ reactivity gain was indicated by this performance (Figure 23).

Two possible mechanisms for reactivity gain were examined in attempting to explain the unexpected behavior. Hydrogen redistribution, as previously mentioned, exhibits a small positive effect upon certain temperature changes. A HYTRAN calculation was performed which indicated a + 0.002¢ effect, which rapidly became negative and at 72 hr was about -0.2¢. Although HYTRAN is acknowledged to be inaccurate during the initial phase of redistribution, it is quite unlikely that the positive redistribution effect could be as large as the unexplained effect shown in Figure 23.

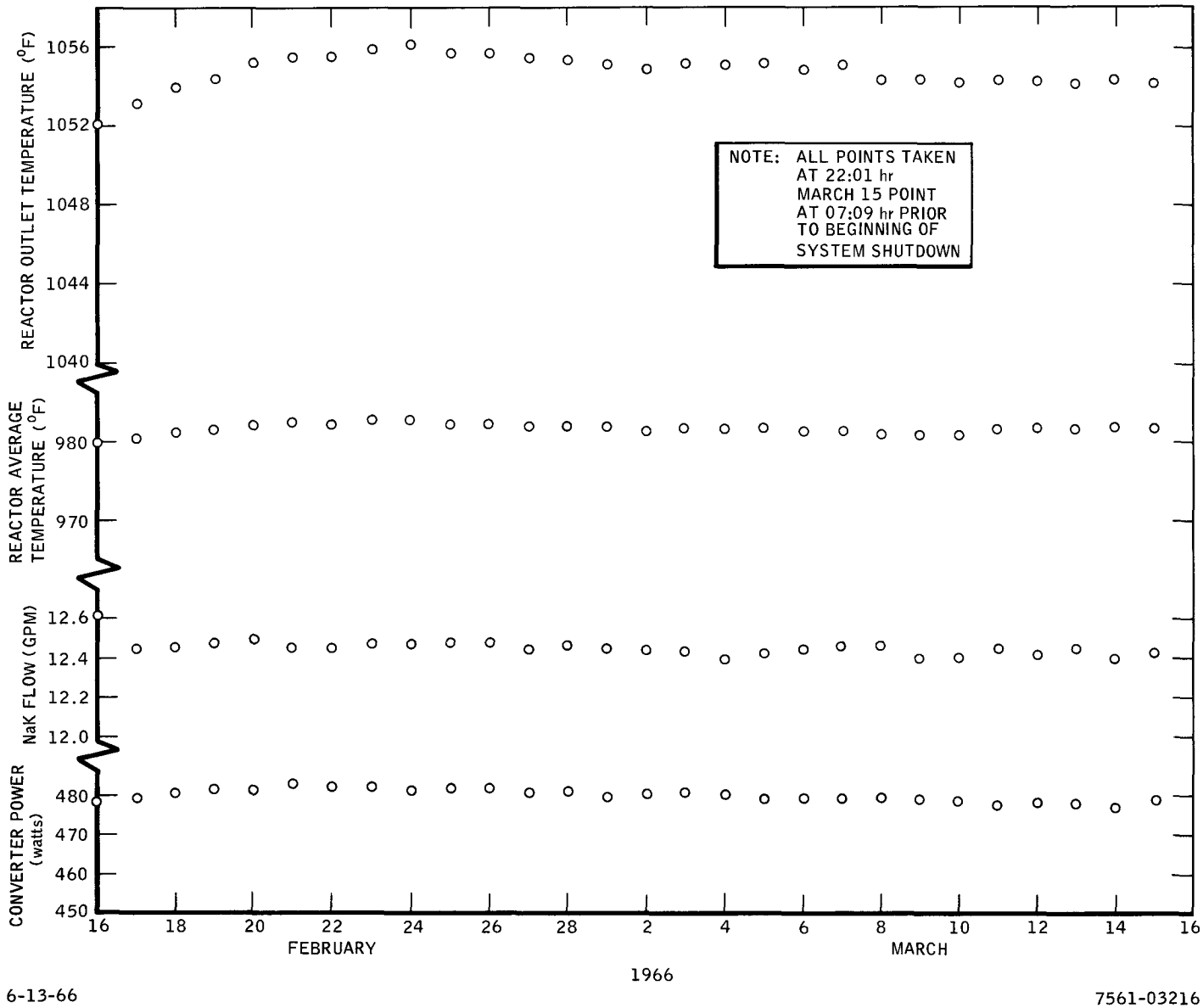

Figure 24. Static Control Performance During Extended Operation Test

It was also speculated that the 54-hr half-life of Pm^{149} may have resulted in an effective high prepoison burnout rate, which might account for the observed reactivity gain. The effect was examined and found to be quite small. A total of + 0.14¢ of net Sm^{149} burnout was calculated to occur between the time of the power change and the time when equilibrium burnout was resumed (about 250 hr).

In summary, the active control phase reactivity losses were significantly (about 3¢) less than expected. No explanation for this performance anomaly has been determined; however, the possibilities of a long-time-constant thermal effect, hydrogen redistribution model error, or some other previously neglected reactivity effect, or effects, have not been fully explored at this time.

3. Static Control Phase

The reactivity gain, mentioned above, continued for about 200 hr until February 24, 1966. Subsequent to that time the power and temperature decreased approximately as predicted. Static control phase performance is shown in Figure 24.

The downward temperature drift was predicted to be about -0.15°F/day using the analytical model described in Section V of this report. The observed drift rate was approximately -0.10°F/day; although the test duration was too short to permit an accurate measurement. At most, the lesser drift rate may be taken as an indication that hydrogen leakage from the FS-3 fuel was not grossly different from the predictions. Hydrogen leakage from intact fuel elements is very temperature dependent, so that high hydrogen loss during the year-long endurance period would have been greatly accelerated by the 73°F temperature increase and the post-perturbation temperature drift rate should have exceeded the nominal predicted rate.

4. Shutdown Phase

Shutdown was initiated by withdrawing the fine control drums, on March 15, 1966. The shutdown was extended over about 20 hr to minimize fuel element damage due to thermal stresses.

Two inverse multiplication (approach-to-critical) experiments were performed about 70 hr after the FS-3 shutdown. Xenon had essentially decayed away by that time, so that a measurement of the cold excess reactivity, and comparison

to the prestartup excess reactivity, should provide an indication of the total unrecoverable reactivity losses incurred during the 10,000 hr of full power operation.

The measured excess reactivity, corrected to the prestartup temperature, was \$2.76 ± \$0.05, compared to the prestartup measurement of \$2.95 ± \$0.05. The apparent net reactivity loss was \$0.19 ± \$0.07.

This measurement was verified by adding the 17.4¢ reactivity lost during the power increase to the unrecoverable active control period losses, and including losses during the static control phase of the perturbation test. The sum of these losses should equal the measured unrecoverable reactivity losses reflected in the change in excess reactivity. The sum was \$0.20 ± \$0.01, which agrees very well with the loss indicated by the excess reactivity measurements.

B. CONTROL SYSTEM PERFORMANCE

The fine control drums were moved successfully after over 1 year of dwell at the position reached at the end of the active control period. The fine control drum actuators operated at a temperature of approximately 525° throughout the test. Satisfactory control drum operation was thus demonstrated in both the active and passive modes (the daily coarse control drum actuator checks) for an endurance period of greater than 1 year. During this period the actuators received a total integrated neutron flux of approximately 1.5×10^{19} nvt and a gamma dose of approximately 1.5×10^{10} r.

After the vacuum chamber was opened following shutdown, the electrically actuated band release device (EABRD) was energized. TV coverage showed that the device actuated properly and the reflector retainer band snapped apart quickly and cleanly. The snap action of the band indicated that the band springs were still exerting considerable tension. Records of the voltage and current to the device showed that it separated after the circuit had absorbed about 2300 watt-sec and that the time to separation was 9-sec. This performance is typical of the performance of new EABRD's and indicates no significant effect from the extended thermal-vacuum-irradiation test.

The discussion of temperature detector performance during shutdown was included for editorial reasons in the section on control system performance during the endurance period (V.C.).

C. DIAGNOSTIC SYSTEM PERFORMANCE

The outputs of the position sensor demodulators during the extended operation test are plotted in Figures 25 and 26. No difficulty was experienced in obtaining the desired motion of the drums (hence sensors) even though the latter had been subjected to over 9300 hr at 350°F, and had received an integrated radiation dose of over 1.5×10^{19} nvt fast neutrons, and 1.5×10^{10} r gamma. No significant electrical nor mechanical damage to the sensors was apparent, as evidenced by the position and slope of the data points during the adjustment of the drums.

The shift in calibration from the end of the active control period, January 25, 1965, to the start of the drum motion on February 16, 1966, was gradual (Table 7). The possible reasons for the shift are discussed in Section V-B-2. An important thing to note is the fact that the slope of the output after 1 year is almost identical to its original value indicating that the sensor was not significantly damaged.

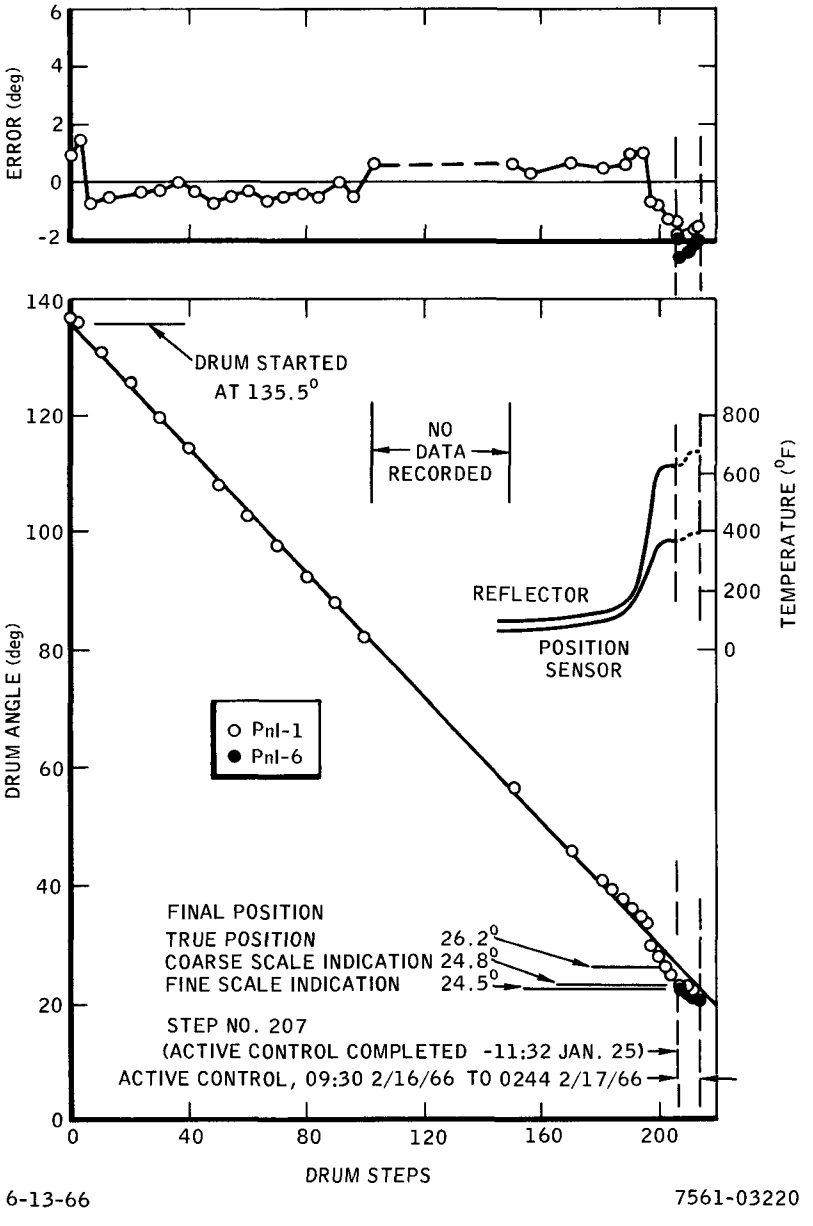

Figure 25. Performance of Coarse and Fine Control Drum No. 3 Position Sensors (Extended Operation Test)

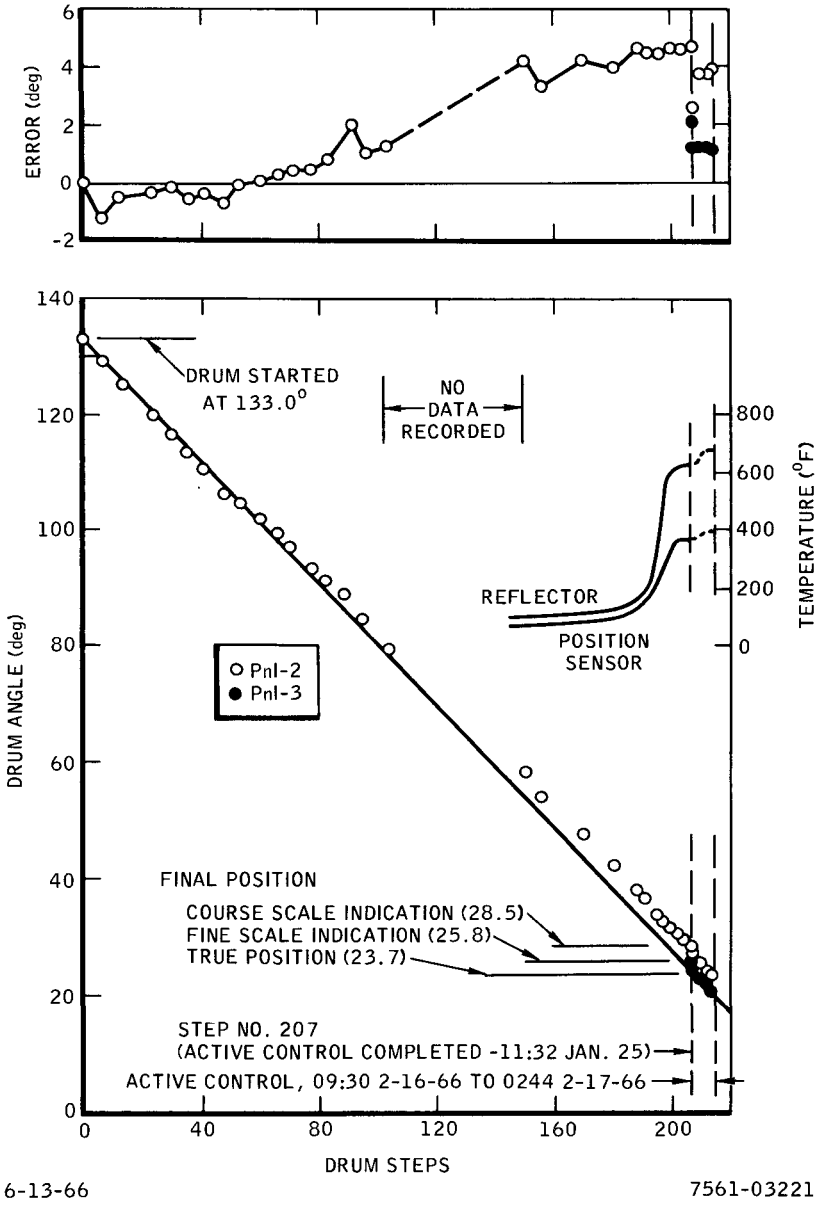

Figure 26. Performance of Coarse and Fine Control Drum No. 4 Position Sensors (Extended Operation Test)

BLANK

VII. CONCLUSION

The FS-3 nuclear ground test verified the SNAP 10A system to be ready for the flight test. Following a series of tests simulating launch conditions the nuclear test successfully demonstrated the automatic startup, short-term active control on outlet temperature, and long-term unattended operation concepts. In addition, the diagnostic instrumentation was shown adequate to provide an analysis of system performance.

During automatic startup, the analytical predictions were shown to be reasonable, and an experimentally determined value for temperature and power defect was established to predict the startup performance of subsequent systems.

For the first time, the ability of the control equipment to bring the system to power and to automatically control power was demonstrated very successfully. The test disclosed the fact that the control system would normally insert two drum steps each time the temperature dropped to the set point during the active control period.

Component temperature values were accurately established for the first time and were near predictions in all cases.

The long-term, unattended operation of the system continued satisfactorily for over a year. It was extremely beneficial in developing a better analytical model for the SNAP zirconium-hydride reactor. The average temperature of the reactor decreased with time through the first 9 months and then held essentially constant at 908°F. This was not as predicted and an intensive analysis was performed to achieve an understanding of the behavior. It was determined that the time required for hydrogen redistribution was much longer than predicted and accounted for most of the difference between the predicted and actual performance. The study of other reactivity effects improved the definition of them, and as a result a much improved reactor analytical model was generated. This new model, which is also based on the SNAP 10A flight reactor (FS-4) performance, provides a close approximation for performance of static-controlled SNAP reactors, particularly those operating in the 1000 to 1100°F temperature range. The model will enable the prepoisoning of future reactors to achieve the designed temperature behavior.

During the early operating period, it appears the test was slightly compromised due to abnormal movement of the reflector resulting from differential thermal expansion. Modifications to the reflector support for remote handling purposes allowed this to happen. The movement was described sufficiently, however, so that the magnitude of its reactivity effect could be calculated. This calculation was shown to be reasonable by the performance of FS-4.

During the last month of operation, the FS-3 system was returned to near its original operating conditions. This provided a gross check of the new analytical model, though the time period was too short to obtain definitive results. This last month of operation was especially important in verifying the component performance after their first test in the true SNAP 10A thermal-radiation environment. All control and diagnostic system components performed satisfactorily. The components located around the reactor had received greater than 1.5×10^{19} nvt and 1.5×10^{10} r at this time.

On March 15, 1966 the scheduled shutdown of the system was accomplished. With 10,005.5 hr of uninterrupted full-power operation the reactor surpassed any other known reactor for length of continuous operation and demonstrated that the SNAP 10A system is capable of long-endurance missions.

[redacted]

REFERENCES

1. R. M. Galantine, et al. NAA-SR-11430, "Preliminary SNAPSHOT-1 Performance Summary" (August 1, 1065)
2. R. B. Paulson and G. Berg, NAA-SR-11934, "Final SNAPSHOT-1 Report," to be published
3. S. Miner, et al. NAA-SR-11206, "Preliminary Test Results - SNAP 10A-FS-3" (September 1, 1965)
4. R. W. Winson, NAA-SR-7322, "HYTRAN-A Hydrogen Diffusion Code," (April 16, 1962)
5. H. P. Flatt and D. P. Satkus, NAA Program Description, "SIZZLE" February 1961, (Internal Document)
6. G. D. Joanou, et al., GA-2451 (Vol. I-IV), "Nuclear Data for GAM-1 Data Tape" (August 22, 1961)
7. J. D. Garrison and B. W. Roos, Nuclear Science and Engineering, Volume 12, pps. 115-134, "Fission-Product Capture Cross Sections" (1962)
8. H. P. Flatt and D. C. Baller, NAA Program Description, "The AIM-6 Code" (January 1961) (Internal Document)
9. R. H. Norman, NAA-SR-TDR-8274, "A Multigroup Library of Absorption Cross Sections for Natural Samarium in Zirconium Hydride Moderated Reactors" (March 21, 1963)
10. J. P. Beall and M. W. Hulin (Editors), NAA-SR-7088, "The Final Report on the SNAP-2 Experimental Reactor (SER) Operation and Test Program" (April 30, 1962)
11. L. D. Felten, et al., NAA-SR-8295, "Final Report on the SNAP-2 Development Reactor (S2DR) Test Program" (April 3, 1964)
12. L. M. Fead et al., NAA-SR-10903, "SNAP-8 Experimental Reactor Operations and Test Results" (June 28, 1965)
13. C. E. Johnson, NAA-SR-11092, "SNAP-8 Progress Report-February-April, 1965" (June 15, 1965)
14. D. W. Clifford, NAA-SR-8613, "Final Report on the SNAP-10A Prototype Critical Assembly Studies" (April 30, 1964)
15. J. Miller, et al., NAA-SR-7140, "Temperature Coefficients and Spectra in the Hydride Moderated SNAP Reactors" (December 30, 1962)
16. J. R. Beyster, et al., Nuclear Science and Engineering, Volume 9, pps. 168-184, "Measurement of Neutron Spectra in Water, Polyethylene and Zirconium Hydride" (February 1961)
17. J. C. Young, et al., Nuclear Science and Engineering, Volume 19, pps. 230-241, "Neutron Thermalization in Zirconium Hydride" (June 1964)

[redacted]

18. W. A. Rhoades, NAA-SR-MEMO-7515, "The QUICKIE Code - A Multigroup Reactivity Calculation for One-Region Systems" (June 22, 1962)

19. E. A. Nephew, ORNL-2869, "Thermal and Resonance Absorption Cross Sections of the U^{233}, U^{235} and Pu^{239} Fission Products" (March 1, 1960)

20. C. W. Hamil and F. B. Waldrop, Y-1454, "Shielding Studies: Neutron Irradiation Damage to Lithium Hydride Compact" (November 11, 1963)

21. R. E. Taylor and C. J. Ambrose, NAA-SR-9782, "Thermophysical Properties of SNAP Fuels" (June 26, 1964)

APPENDIX A
ABNORMAL REFLECTOR MOVEMENT IN S10FS-3

Several modifications of the FS-3 reflector mounting were made to allow for remote removal of the reflector. As a result of these modifications, it was possible for the reflector blocks to move relative to the reactor vessel in an abnormal manner. The possibility of this was first recognized when limit switches indicated reflector ejection during startup. This movement is especially important since reactivity effects have been postulated as a result of the movement. The thermal and mechanical calculations supporting the reflector motion theory are presented in this appendix, while the magnitudes of the reactivity effects are discussed in the sections on nuclear or reactor performance.

The reflector position indicating limit switches, PnS-15 and PnS-16 gave indications of "Reflector-off" shortly after the start of the reactor heatup ramp. The events recorded are as follows:

1) PnS-15 (+Z Reflector ON-OFF)

At 1322 on January 22, 1965, this switch actuated (closed) and remained closed until approximately 0600 on January 23, 1965, when it switched (open).

2) PnS-16 (-Z Reflector ON-OFF)

At 1334 on January 22, 1965, this switch actuated (closed) and remained closed for 100 days. It switched (open) on May 2, 1965.

At 1322 and 1334 the reactor outlet temperatures were approximately 370 and 430°, respectively. The reflector thermocouples, TC-31 and TC-40, showed no significant rise above the 85°F ambient condition at that time.

The last setting on these switches was made when the system was in the chamber after the switches had been removed to allow operations personnel to install some remote handling equipment. They were set at an overtravel of 0.015 to 0.020 in. established by measuring the clearance between the actuator and the switch case. The differential travel on these switches varies from 0.008 to 0.011 in. The overtravel setting and the switch differential travel would require a 0.023 to 0.031 in. relative movement between the reflector and vessel before switch actuation.

The fact that both switches actuated within a very short time interval (12 min), at a time when the reflector had not changed temperature and the core temperature was rising and the vessel was therefore expanding, indicates that the switches actuated because the reflectors were moving upward relative to the lower end of the vessel. The vertical differential expansion between the reflector and vessel when the first switch actuated was calculated to be 0.042 in. and was 0.051 in. when the second switch actuated. If there were little or no relative motion between the reflector and vessel at the upper contact point, the limit switches could easily have actuated.

On FS-3 the reflector ejection springs and the hinge eccentric pins were omitted to facilitate remote removal of the reflectors at the end of the test. There was, therefore, nothing other than gravity to prevent upward movement of the reflectors. Upward forces would occur from frictional forces between the reflector top positioning bolts and the reflector upper stops. These frictional forces are due to the pressure of the reflector band tension.

A force analysis of a reflector half (Figure A-1), which takes into account the reflector weight, reflector band tension, and the forces applied by the sash weight reflector ejectors, shows that a 63-lb upward force is required to lift a reflector half and that the coefficient of friction between the positioning bolts and the stops would have to be 0.49 or greater, assuming the frictional forces at the lower hinge to be negligible.

A second calculation was made assuming that the coefficient of friction at the upper contacts and at the hinges was identical. This assumption requires a friction coefficient in the range of 0.85 to 1.54 for liftoff. Values below this range would not develop a large enough upward force at the upper contact to overcome reflector and sash weight and the resisting lower contact friction. Values above this range would cause the reflector to pivot about the lower contact and subsequently decrease the upper contact pressure and resultant upward force.

The coefficient of friction range for the materials concerned is 0.55 to 1.00, and possibly higher. Thus in the first assumption above, the frictional forces are more than adequate to cause liftoff. For the second assumption, the forces are in the range required to result in liftoff.

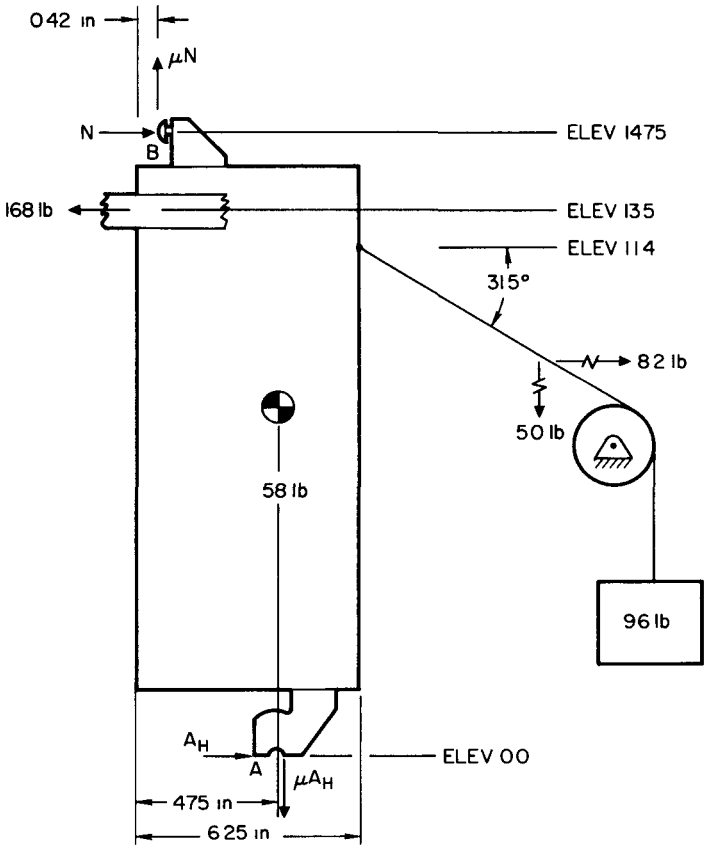

CASE NO 1 IF μ AT A = 0 N = 128 lb AND μ AT B = 0 49
CASE NO 2 IF μ AT A = μ AT B 085 < μ < 154

5-18-65 7623-0581

Figure A-1. Force Analysis of S10FS-3 Reflector

Other possible sources of lifting force on the reflector were considered. The reflector band will develop an upward force vector between the dummy TABRD and the standoffs, which in this case are the bearing brackets. The band reach on each side is approximately 5-1/2 in. and, with an 80-lb band tension, the upward vector is about 2 lb when the TABRD rises 0.050 in. relative to the reflector.

The lower cable bundles of the reflector wiring harnesses constitute another possible source of upward pressure. These bundles come off the reflector at an inward angle and make a tight turn outward, exerting some pressure on the top surface of the shield, and then curve down to the interface receptacles. These bundles are very stiff and not very elastic and therefore could cause a

significant upward force which would diminish very rapidly as the reflector moved upward. This analysis is partially contradicted by the fact that, at the time switch acutation occurred, the bottom of the reactor was probably rising relative to the top surface of the shield due to heating of the reactor support legs by the coolant inlet and outlet pipes.

Additional analyses were made to establish in greater detail the possible movements of the reflectors relative to the core during the temperature transients of startup and the first few hours of the active control period. Of particular interest, because they would affect reactivity, were the possible movements of the bottom of the reflectors towards and away from the core.

Figure A-2 shows the temperatures of the reactor core vessel and the reflector assembly during startup and the first few hours of active control.

As the reactor temperature increases the reflector is pulled up and pivots at the upper contacts. The lower end moves vertically up and horizontally inward around the hinge pin. The horizontal movement is limited to approximately 0.050 in. At this point, the reflector inside diameter contacts the vessel wall permitting further motion only in the vertical direction. It is therefore possible for a gap to exist between the hinge and pin for about 1-1/2 hr commencing approximately 1-1/2 hr after startup. Figure A-3 shows movement of the reflector hinge based on the assumption that no slippage occurs at the upper reflector-to-vessel contacts.

Three hours after startup, the hinge should again contact the pin due to increasing reflector temperature and downward expansion of the reflector

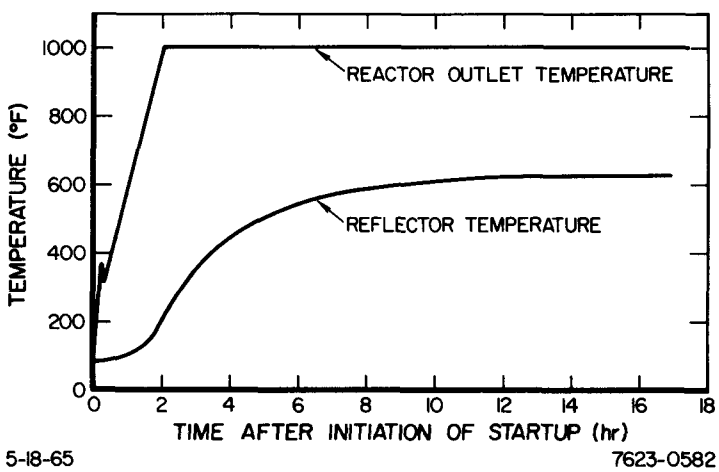

Figure A-2. Reflector and Reactor Vessel Temperature Transients

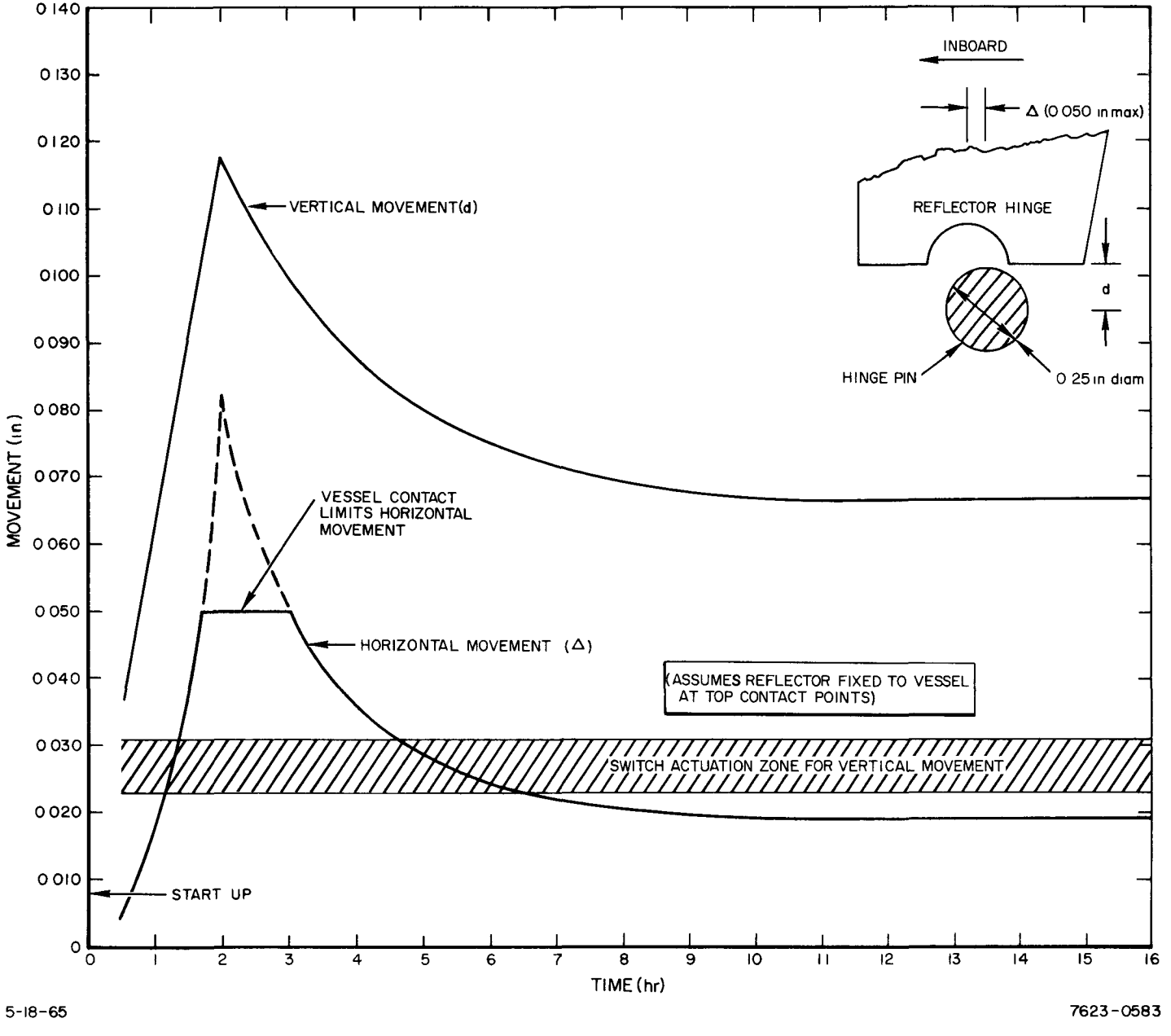

Figure A-3. Analysis of Reflector Movement Relative to Hinge Pin

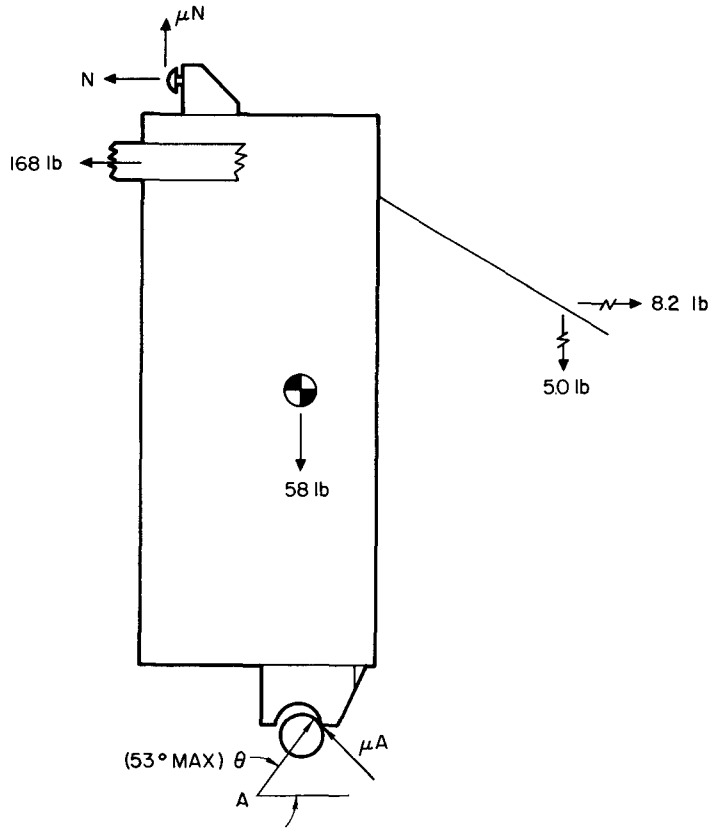

Figure A-4. Hinge Pin Force Analysis

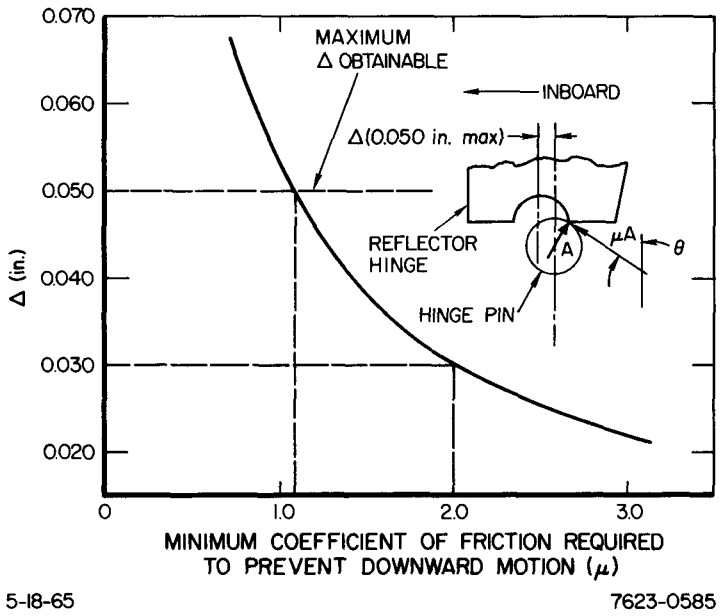

Figure A-5. Friction Coefficient to Prevent Reflector Motion vs Horizontal Displacement

relative to the vessel upper contact. At the instant of contact, forces begin to develop which tend to resist the return of the reflector to its normal position. These forces are the normal and frictional resistance of the edge of the hinge bearing on the pin (Figure A-4). Based on the assumption that the frictional value is equal at all contacts, values of the friction coefficient were determined which would prevent further downward motion of the reflector blocks. These values are shown as a function of horizontal displacement in Figure A-5.

The maximum inboard location of the hinge axis with respect to the pin axis (Δ) is 0.050 in. Figure A-5 shows that, for this position, the minimum coefficient of friction required to prevent downward movement of the hinge around the pin is 1.09. If the value actually developed at the hinge contact should exceed this value, the reflector would slip at the upper contact preventing downward motion and the base of the reflector would remain at the 0.050 in. inboard location. A second example (Figure A-5) indicates that, for a Δ of 0.030 in., a coefficient of friction of 2.00 or less would permit downward motion of the reflector.

Since the frictional values involved are thought to be less than the values required to prevent the downward movement of the reflector, it is to be expected that the sliding of the hinges around the pins would occur thereby allowing the return of the reflector to its normal position. The reactuation of the ejection switches (noted at the beginning of this Appendix) indicates that the reflector halves did reseat on the hinge pins.

The possibility of reflector movement was verified in a non-nuclear thermal test simulating the FS-3 startup. Modifications identical to those made on FS-3 were made to a reflector and vessel, the two were assembled into the thermal-vacuum acceptance test chamber, and heaters were installed in the vessel. During a first simulated startup, neither optical measurements nor limit switch actuations indicated any abnormal reflector motion. Prior to a second test, the reflector retainer band tension was increased from 80 lb, as on FS-3, to 105 lb. During the second test, then, both the optical instruments and limit switches did indicate the abnormal lifting and inward motion of both reflector halves. The halves moved upward 0.028 in. during the latter part of the temperature ramp, then the hinges returned to 0.015 in. above their pins as the reflector heated and expanded. Movement of the control drums caused the

halves to drop back onto the hinge pins. It was concluded from these tests that the postulated reflector motion could occur and that it would be indicated by the limit switches. Also, drum movement could trigger downward and outward motions of a cocked reflector.

In summary, it is apparent that the modifications made to the FS-3 reflector mounting to permit remote handling allowed abnormal movement of the reflector, especially during periods of thermal transient. The primary indication of movement was the unexpected and erroneous indications from the two reflector ejection limit switches during startup. Analyses of the differential expansion during the startup period and the forces on the reflector showed that the movement was possible. This was demonstrated by a non-nuclear thermal test simulating the FS-3 startup. The reactivity effects associated with this abnormal movement are discussed in the sections of this report dealing with nuclear or reactor performance (Sections III-B, IV-B, and V-A).

APPENDIX B

STATIC CONTROL BEHAVIOR FOR HIGH-TEMPERATURE HIGH-POWER SNAP REACTOR OPERATION

The uncertainties in magnitude of individual reactivity effects associated with operation of SNAP reactors at higher powers and temperatures are greater than in FS-3. The net reactivity uncertainty, although greater than at lower temperatures, is not as large as one might expect by considering the reactivity effects individually, however. This is because the errors in reactivity predictions are considerably damped by the strong temperature dependence of hydrogen leakage. Figure B-1 is a typical example of this dependence. It is seen that the leakage rate approximately doubles with a 50°F increase in reactor temperature. If reactivity losses under static control are greater than predicted, the reactor temperature will tend to be lower than predicted. This lower temperature in turn causes the hydrogen leakage rate to be less and, therefore, the total reactivity loss rate is decreased. The effect of the temperature dependence of hydrogen leakage, then, is to decrease the temperature drifts due to errors in reactivity predictions. In 1000°F operation, such as FS-3, this effect is not significant due to the smaller magnitude of hydrogen leakage (about $0.03 in a year, less than a tenth of the static control period loss, as opposed to $2.00-$4.00 at elevated temperatures, which is about four times the other long-term losses).

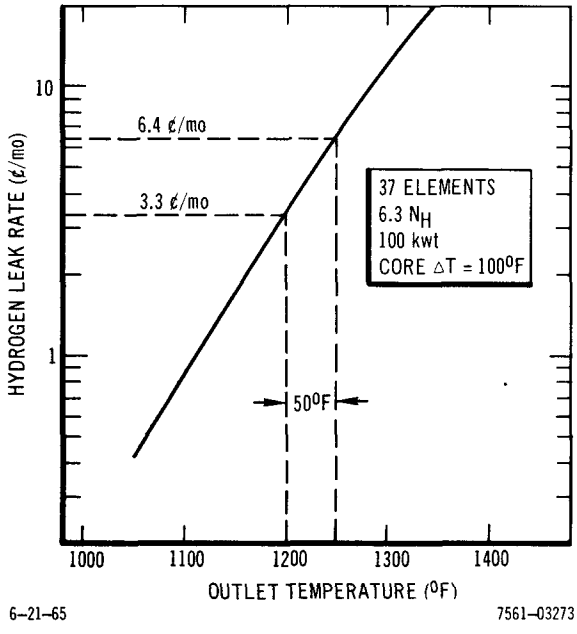

Figure B-1. Dependence of Hydrogen Leakage Rate on Temperature

For convenience in illustrating the static control behavior at elevated power and temperatures, a comparison will be made between the FS-3 design and one particular high-temperature reactor (Table B-1).

TABLE B-1

REFERENCE 1300°F REACTOR DESIGN
FOR PERFORMANCE COMPARISONS

Core Diameter (in.)	8.875
Core Length (in.)	12.25
Number of Elements	85
Thermal Power (kw)	100
Coolant Outlet Temperature (°F)	1300
Core ΔT (°F)	190
Operating Life (years)	3

The discussed reactor, similar to one which might be proposed for a communications satellite, was selected as an example because of the amount of analysis performed on it to date. Although the design life for this reactor is 3 years, the end-of-life temperature uncertainties are only slightly reduced for a reactor designed for a 1-year operating period. Comparisons of various uncertainties are discussed in the following text.

A. PRIMARY PERFORMANCE UNCERTAINTIES

1. Hydrogen Loss

The major reactivity loss in the example is due to hydrogen loss. At present, this effect also has the greatest uncertainty in calculation. Nominal hydrogen leakage can be calculated by the LOAFER code using extrapolations from isothermal out-of-pile permeation tests. (The LOAFER code is a stepwise calculation in time of hydrogen leakage, reactivity and reactor temperature. The HYLO code is incorporated as a subroutine for hydrogen leakage calculations.) Existing experimental data (S2DR, S8ER) have shown, however, that in-core hydrogen leakage rates are greater than extrapolated from out-of-pile tests. At first glance, this seems to make static control at elevated temperatures impossible. If nominal hydrogen leakage were $2.00 in the reference reactor, for example, and if the initial leak rate was actually three times nominal, it might be calculated that actual hydrogen leakage should be $6.00. Since this

would be $4.00 greater than expected, the end-of-life temperature might be several hundred degrees lower than expected, thereby invalidating the concept of high temperature static control.

This analysis, however, ignores the effects of temperature dependency of hydrogen leak rate and of depletion of hydrogen. An example of these effects is given in Figure B-2. This figure shows the factor by which the leakage throughout the reactor design life (integrated leakage) is increased by errors in predicted initial leak rate. In the curve, labeled "Active Control," the effects of hydrogen depletion are illustrated. In this case it is assumed that the control system holds the temperature constant. It is seen that the integrated leakage does not increase linearly with initial leak rate due to the drop in hydrogen pressure driving force accompanying hydrogen depletion. For example, should the initial leak rate be three times nominal, the integrated leakage is increased only by a factor of 2.27. The most powerful effect, however, is that due to the temperature dependency of leak rate. The curve marked "Static Control" allows the temperature to drop to compensate for the increased leakage. The drop in temperature causes a decrease in integrated leakage below what would be obtained were the temperature held constant as in active control.

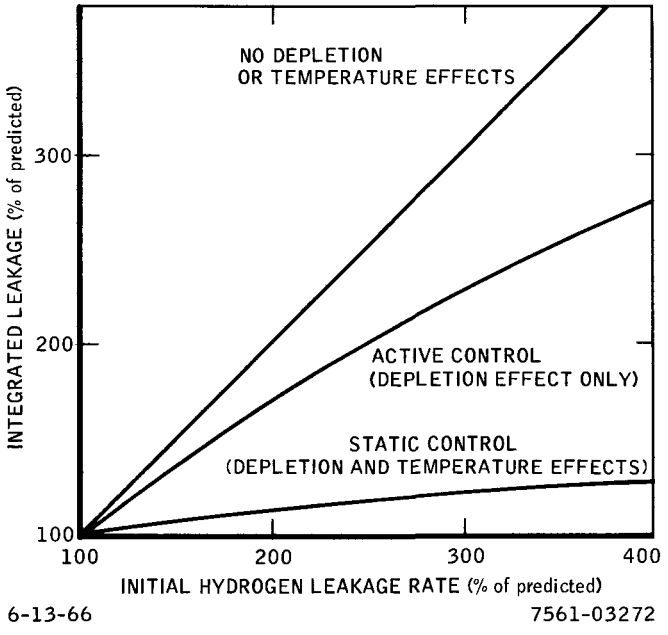

Figure B-2. Hydrogen Leakage (Time Integrated) vs Leakage Rate

In the case just discussed, of an initial leak rate three times nominal, for example, the integrated leakage would increase by a factor of only 1.22. The accompanying temperature decrease would only be 70°F instead of the hundreds of degrees drift which would be present should neither effect exist.

A study was performed to determine the uncertainty in initial hydrogen leak rate which could exist without causing an excessive degree of end-of-life uncertainty. It was found that if this initial rate could be determined to within a factor of about 2 (i.e., the ratio of maximum to minimum possible values is less than 2), the resultant end-of-life uncertainty due to integrated hydrogen leakage could be made less than ±26°F by loading a prepoison designed for an initial leakage rate in the middle of the uncertainty band. An important additional finding was that the end-of-life temperature uncertainty due to hydrogen leakage is virtually independent of the absolute level of hydrogen leakage rate so long as the initial rate is known within a factor of 2 (maximum-to-minimum).

Limiting the assumed uncertainty in initial hydrogen loss rate to within a factor of 2 between minimum and maximum possible values is judged to be a reasonable criteria for design of static control reactors. This criteria can be approached with additional in-pile tests and with further evaluation of FS-3 performance. This criterion is basically considered, however, as applying to the second reactor in a series, i.e., the hydrogen loss rate is determined empirically by operation of the first reactor either on the ground or in orbit. For the first reactor in a series, the end-of-life temperature uncertainty due to errors in prediction of hydrogen loss rate would be approximately double the ±26°F uncertainty discussed in this section.

2. Hydrogen Redistribution

Uncertainties in the time behavior of this phenomenon, which contributed a large uncertainty in FS-3 operation, should not be significant in elevated temperature operation. Because of the increase in hydrogen diffusion rates through the fuel material with temperature, equilibrium hydrogen redistribution is attained in much shorter time periods than in FS-3. The entire magnitude of redistribution would be compensated during a 3- to 4-day active control period at 1300°F. Recent experiments in the S8ER have shown a redistribution time constant of about 20 hr at 1300°F.

The uncertainty in magnitude of additional hydrogen redistribution resulting from deviations from nominal performance is included as part of the uncertainty attributed to the reactivity loss mechanism causing the off-nominal performance.

3. Prepoison Uncertainities

The effect of prepoison uncertainties on the end-of-life temperature of the subject reactor can best be illustrated by an example. The example can also show the effect of an equivalent uncertainty on a reactor at SNAP 10A conditions. The illustration is summarized in Table B-2 following the discussion.

TABLE B-2

ILLUSTRATION OF EFFECT OF UNCERTAINTY IN PREPOISON BURNOUT

	1300°F Reactor			SNAP 10A		
	Minimum	Nominal	Maximum	Minimum	Nominal	Maximum
Prepoison Loading Worth at Temperature ($)	7.25	8.28	9.31	1.19	1.39	1.59
Reactivity Gain During Design ($) Life (prepoison burnout less fission product Sm^{149} buildup)	3.87	4.67	5.47	0.027	0.086	0.145
Possible Deviation in Reactivity Gain ($)	-0.80		+0.80	-0.059		+0.059
Gross Temperature Uncertainty for Prepoison Burnout (°F)	-267		+267	-20		+20
Integrated Hydrogen Leakage Worth with Nominal Initial Loss Rate ($)	3.00	3.70	4.40	0.027	0.030	0.033
Reactivity Gain less H Leakage Worth ($)	0.87	0.97	1.07	0.000	0.056	0.112
Possible Deviation in (Gain less Leakage Worth) ($)	-0.10		+0.10	-0.056		+0.056
Net Temperature Uncertainty for Prepoison Burnout (°F)	-33		+33	-19		+19

The worth of the SNAP 10A prepoison loading, Sm_2O_3, based on experimental measurements was determined to be \$1.55 ± \$0.20. The uncertainty of ±13% was due to the scatter of measured values for Sm_2O_3 worth on fuel elements. The amount of prepoison (Gd^{155}), required in the 1300°F reactor is \$9.20. Because of the larger amount, the accuracy of the measurement in a critical assembly should be better percentagewise. A conservative estimate for this case is ±10% or ±\$0.92.

Additional uncertainty in the worth of the prepoison loadings at operating temperature may be introduced by errors in prediction of neutron spectral effects. In SNAP 10A the change in worth of the prepoison due to a shift in neutron spectrum when raising the temperature to operating conditions was assumed to be -10% ±5%. In spite of the higher temperature in the 1300°F reactor, the same estimate is good since the spectrum does not affect the Gd cross section as strongly as the Sm cross section.

Applying the 10% reduction in worth and combining the uncertainties in loading worth and spectral shift statistically, the initial loading worth at temperature is found to be \$1.39 ± 0.20 for SNAP 10A and \$8.28 ± 1.03 for the 1300°F reactor. The reactivity gain due to prepoison burnout during the reactor life, allowing for the dependence of burnout rate on the magnitude of spectral shift, is calculated to be 8.6¢ ± 5.9¢ for SNAP 10A and \$5.71 ± 0.80 for the 1300°F case. To make these numbers consistent, the 1300°F reactor gain value should be reduced by the amount of fission product Sm^{149} formed during the design life, \$1.04 ± 0.01. The comparable reactivity gain is, then, \$4.67 ± 0.80.

The ±5.9¢ uncertainty in reactivity gain on SNAP 10A is equivalent to ±20°F in average temperature. The ±80¢ in the 1300°F case would be equivalent to ±267°F. This does not consider the effect of associated changes in hydrogen loss rate, however.

The worth of the nominal integrated hydrogen leakage for SNAP 10A is -3¢. If the reactivity gain was at the minimum in this reactor, causing the temperature to drift lower than expected, the hydrogen loss rate would decrease and the integrated leakage throughout the design life would be only -2.7¢. Subtracting this 0.3¢ change in leakage from the -5.9¢ uncertainty leaves -5.6¢ or -19°F as the net effective uncertainty in end-of-life temperature.

For the 1300°F reactor the worth of the nominal integrated hydrogen leakage is -$3.70. In this case if the reactivity gain was minimum, the leakage would be reduced to -$3.00 by the effect of falling temperature. Subtracting the difference in leakage of 70¢ from the -80¢ uncertainty leaves only -10¢ or -33°F as the net effective uncertainty in end-of-life temperature.

In conclusion, the net end-of-life temperature uncertainty (as affected by prepoison burnout and hydrogen loss) is increased from ±19°F on SNAP 10A to only ±33°F on the subject 1300°F reactor, due to the beneficial effect of temperature dependence of hydrogen leakage. Similar illustrations could be presented in the following sections to support the estimates of net end-of-life temperature uncertainty quoted for the other individual reactivity loss mechanisms.

B. OTHER CONTRIBUTING EFFECTS

1. Reflector Motion

This effect was unique in FS-3 due to special ground handling provisions and would not apply to future reactors.

2. Fuel Burnup and Fission Product Accumulation

If the 20% uncertainty applied to FS-3 analysis is used directly in analysis for the high temperature reactor, an end-of-life temperature uncertainty of about ±9°F results. This is the net end-of-life uncertainty after allowing for the temperature dependence of hydrogen leakage.

3. Radiation Damage

These effects were minor during FS-3 operation and are not expected to increase significantly in spite of the higher temperatures. Their maximum contribution to FS-3 uncertainty was about ±4°F. With an increase in these effects by a factor of 5, to allow for the 2.5-fold increase in power and higher temperature, the dampening effect of hydrogen leakage temperature dependence will still maintain the net temperature uncertainty at ±6°F.

4. Thermal Effects

Changes in heat transfer properties and flow patterns influence end-of-life uncertainty by their effect on fuel temperatures and ultimately hydrogen leakage rates. FS-3 analysis has shown that the effects of hydrogen redistribution could have increased the heat transfer resistance between fuel and coolant by

at most 5% due to fuel material shrinking and a resultant increase in the gas gap between the fuel and cladding. Because of the higher temperatures involved leading to fuel swelling and the scarcity of data at higher temperatures, the resistance may change during the reactor's lifetime by as much as 15%. This uncertainty leads to a net end-of-life temperature uncertainty of about 6°F.

C. PREDICTED PERFORMANCE

The predicted contributions to end-of-life temperature uncertainties for the 1300°F reactor are repeated in Table B-3 with a comparison to the analagous values for SNAP 10A.

TABLE B-3

COMPARISON OF END-OF-LIFE TEMPERATURE UNCERTAINTIES BETWEEN A 1300°F REACTOR AND SNAP 10A

	1300°F Reactor	SNAP 10A*
Hydrogen Leakage	±26°F	+0 / -21 °F
Hydrogen Redistribution	-	±21
Prepoison Burnout	±33	±20
Fission Products and Fuel Depletion	±9	±9
Radiation Damage	±6	±3
Thermal Effects	±6	+0 / -1
Net Effect	±44	+29 / -35

*Reflector slippage not considered — FS-3 only.

The net effect shown was determined, assuming the effects were independent, by taking the square root of the sum of the squares of the individual contributions. As stated previously, even though the 1300°F reactor uncertainties are for a 3-year design life, they are only slightly greater than the uncertainties for a 1300°F reactor designed and prepoisoned for 1-year life.

D. CONCLUSIONS

SNAP 10A FS-3 operation has provided invaluable information regarding statically controlled reactor operation with which the behavior of 1000°F, SNAP 10A type reactors can be accurately predicted empirically. Information derived from the FS-4 system corroborates data received from FS-3. The significance associated with the similarity of the behavior of FS-3 and FS-4 is the the clear indication that observable random reactivity effects are not present in SNAP 10A reactor operation.

The magnitude of the temperature uncertainties associated with statically controlled reactors operating at higher power levels and higher temperatures than SNAP 10A will not be proportionally greater than the uncertainties at 1000°F and 40 kwt for several reasons. The hydrogen redistribution effect is essentially completed during the active control period for high-temperature reactors; all uncertainties are reduced by the strong temperature dependency of the overriding loss mechanism, hydrogen leakage; prepoison uncertainties are further minimized due to the larger amount of poisons required for the higher powered conditions; and improved analytical techniques have been developed which account for effects which were previously not taken into account. Based on the above, it is our conclusion that statically controlled reactor systems can be built and their behavior accurately predicted.